catalysts

MDPI

Review

Recent Advances in the Design and Photocatalytic Enhanced Performance of Gold Plasmonic Nanostructures Decorated with Non-Titania Based Semiconductor Hetero-Nanoarchitectures

Jose I. Garcia-Peiro [1,2,3], Javier Bonet-Aleta [1,2,3], Carlos J. Bueno-Alejo [4] and Jose L. Hueso [1,2,3,*]

[1] Instituto de Nanociencia y Materiales de Aragon (INMA), CSIC-Universidad de Zaragoza, 50009 Zaragoza, Spain; joseignacio.garcia.peiro@gmail.com (J.I.G.-P.); jbaleta@unizar.es (J.B.-A.)
[2] Department of Chemical Engineering and Environmental Technology (IQTMA), University of Zaragoza, 50018 Zaragoza, Spain
[3] Networking Research Center on Bioengineering Biomaterials and Nanomedicine (CIBER-BBN), 28029 Madrid, Spain
[4] Department of Chemistry and Molecular and Cell Biology, University of Leicester, Leicester LE1 7RH, UK; carlosj_bueno@yahoo.es
* Correspondence: jlhueso@unizar.es; Tel.: +34-876555442

Received: 3 November 2020; Accepted: 9 December 2020; Published: 14 December 2020

Abstract: Plasmonic photocatalysts combining metallic nanoparticles and semiconductors have been aimed as versatile alternatives to drive light-assisted catalytic chemical reactions beyond the ultraviolet (UV) regions, and overcome one of the major drawbacks of the most exploited photocatalysts (TiO_2 or ZnO). The strong size and morphology dependence of metallic nanostructures to tune their visible to near-infrared (vis-NIR) light harvesting capabilities has been combined with the design of a wide variety of architectures for the semiconductor supports to promote the selective activity of specific crystallographic facets. The search for efficient heterojunctions has been subjected to numerous studies, especially those involving gold nanostructures and titania semiconductors. In the present review, we paid special attention to the most recent advances in the design of gold-semiconductor hetero-nanostructures including emerging metal oxides such as cerium oxide or copper oxide (CeO_2 or Cu_2O) or metal chalcogenides such as copper sulfide or cadmium sulfides (CuS or CdS). These alternative hybrid materials were thoroughly built in past years to target research fields of strong impact, such as solar energy conversion, water splitting, environmental chemistry, or nanomedicine. Herein, we evaluate the influence of tuning the morphologies of the plasmonic gold nanostructures or the semiconductor interacting structures, and how these variations in geometry, either individual or combined, have a significant influence on the final photocatalytic performance.

Keywords: plasmonics; photocatalysis; heterostructures; semiconductors; NIR; core-shell; Janus-like; yolk-shell; nanorods; chalcogenides

1. Introduction

Since the first reported example of heterogeneous photocatalysis in 1911 applied to the degradation of Prussian Blue by ZnO powder and illumination [1], the degree of sophistication and complexity in photocatalyst design has experienced a huge development [2]. In heterogeneous photocatalysis, the process is initiated by the interaction between incident photons and the catalyst. The photon absorption by the catalyst (typically a semiconductor) leads to the promotion of valence band electrons into the conduction band, thereby creating electron-hole pairs. Those carriers can induce the subsequent generation of free radicals (e.g., hydroxyl (OH), superoxide (O_2^-)) to target specific chemical reactions. As a requirement, the energy of the incident photon (hν) must be equal or higher than the energy band gap (E_g) of the catalyst, meaning that the incident electromagnetic wavelength must be energetic enough to overcome the barrier to excite an electron from the highest occupied energy levels to the lowest unoccupied levels. Well-established semiconductor-based photocatalysts, such as TiO_2 or ZnO possess high E_g values (3.05 [3] and 3.3 [4] eV, respectively) and are constrained to the more energetic ranges of the solar spectrum (i.e., UV window representing only up to 5% of the solar radiation) for an effective photoactivation. Abundant efforts have been devoted in the past decades to expand the photocatalytic response of heterogeneous semiconductor photocatalysts towards the visible and infrared ranges in order to maximize the absorption of the solar spectrum [5–9]. One of the most promising and explored strategies has consisted on the combination of semiconductor structures with noble-metal based nanoparticles [10–12]. Recent reviews available in the literature have deepened into the synergistic action of small metal nanoparticles decorating semiconductors and on how the controlled architecture of the latter may have a strong influence on the final photocatalytic outcome [13–20]. Another interesting aspect of metallic nanostructures correlates with their unique optical response that can be modulated upon variations of their specific size and morphology [19–23]. At the interface between the metal surface and other medium (with different dielectric properties), exist a phenomenon known as Localized Surface Plasmon (LSP) that consist on a coherent delocalized electron oscillation leading to the generation of an electromagnetic field both outside and inside the metal. An excitation with radiation of the right wavelength causes a resonance interaction and subsequent collective oscillation of conduction electrons, in the case of metallic materials, due to the restoring force between electrons and nuclei through Coulombic attraction (Figure 1). This phenomenon is called Localized Surface Plasmon Resonance (LSPR), and for metals like Au, Ag, or Cu, the LSPR may take place over a wide range of 400–1300 nm [24] as a function of their size and shape (Figure 1). Thus, metallic nanoparticles emerge as perfect candidates as visible near infrared (NIR) light harvesters to combine and improve the efficiency of semiconductor photocatalysts.

So far, TiO_2 has been set as one of the most explored semiconductors to form hetero-nanostructures in combination with metals to overcome its limited photo-response beyond UV window [25,26] that can overcome its one of the most widely used semiconductors to carry out photocatalytic reactions. Systematic evaluation of Au-TiO_2 hybrid systems exploring the role and influence of shape, specific configuration, heterojunction conformations, and so on, have been developed in the past years. Numerous and varied architecture designs have been successfully reported including core-shell (concentric and eccentric) [27,28], yolk-shell [29], Janus type structures [28], or even multi-component heterostructures [30,31] and their performance successfully tested towards energy and environmental applications [17,18,31–33]. The generation and assembly of these hetero-nanostructures offers multiple advantages but the number of alternative candidates to TiO_2 still remains as an open challenge. The present review intends to overview the most recent advances described in the literature involving the design of hybrid photocatalysts combining plasmonic Au nanoparticles and non-titania based semiconductor coatings organized in a wide variety of nanoarchitectures (vide infra). Herein, we paid special attention to plasmonic hybrids that involved the selection of anisotropic Au nanostructures (mostly nanorods (AuNRs) and nanostars (AuNSs)) and a controlled growth of semiconductors beyond the most typically studied (i.e., TiO_2 [27,34,35] or ZnO [5,36,37]). This approach allows a fine control of sizes for both metal and semiconductor, reduces the probability of recombination of carriers, and maximizes an intimate contact to form efficient heterojunctions [38]. In contrast, other methodologies lack sufficient control on the size and dispersion of metal nanoparticles or the corresponding supports. Furthermore, many times these semiconductor nanoparticle supports require additional tuning or post-treatments to ensure the exposure of preferential facets that do not necessarily prevent numerous bulk recombination events due to their inherent polydispersity [13]. Hence, recent research innovative trends, such as cancer therapy, require more accurate control of the photocatalysts dimension for proper internalization in cells and accurate reproducibility [39]. Therefore, we consider that the efforts made to improve the generation of novel plasmonic photocatalysts with a controlled size and distribution in a core-shell (or analogous nanoarchitecture) and/or semiconductor supports represents a very promising alternative to other metal-semiconductor configurations [13]. Herein, we have made special emphasis on highlighting the latest achievements with AuNRs or AuNSs as plasmonic cores and different oxides (CeO_2 and Cu_2O) or chalcogenide semiconductors (CuS, CdS) grown with core-shell, Janus, or dumbbell-like configurations. We have correlated the influence of the different architectures with their final photocatalytic response.

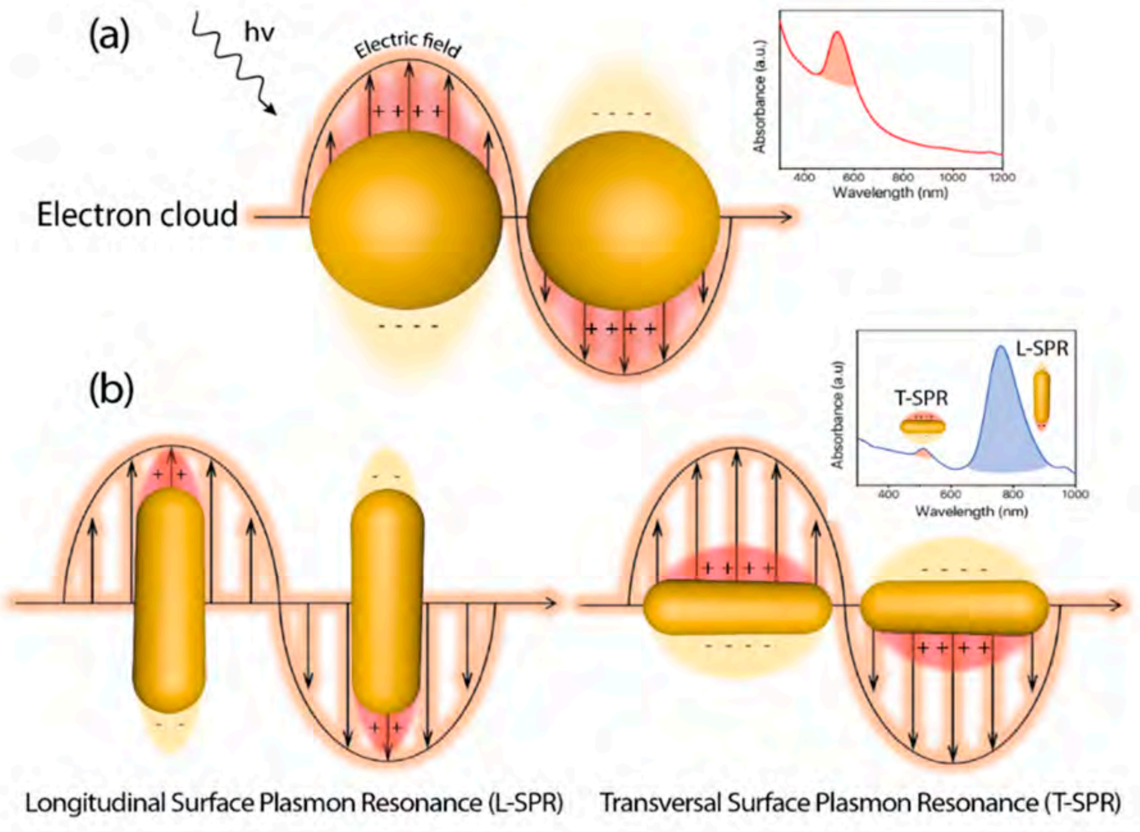

Figure 1. Morphology of the plasmonic nanostructure determines its Localized Surface Plasmon Resonance (LSPR). (**a**) Isotropic Au nanoparticles (AuNPs) possess confined electrons alike in all directions, resulting in a single LSPR band in the visible range; (**b**) the introduction of morphological anisotropy allows LSPR with different absorption maxima. For the particular case of nanorods (AuNR), the longitudinal induced anisotropy entails an LSPR at the near-infrared (NIR) window as the confinement of electrons is different at the AuNR edges or sides.

2. Metal-Semiconductor Hetero-Nanostructures: Different Configurations and Light-Driven Activation Mechanisms

A key feature of plasmonic photocatalysts is related with the photo-induced generation of highly energetic electrons (hot electrons) generated via LSPR [40]. The distribution of these hot electrons can be described by the Fermi equation using an elevated effective temperature [41]. After light absorption, LSPR decay may occur either radiatively, through re-emitted photons, or non-radiatively, for instance through transfer of hot electrons [42], generally through intraband excitations within the conduction band [40,43] thereby causing electrons from occupied energy levels to be excited above the Fermi energy. Hence, after coupling with metals, typical semiconductors used in photocatalysis can capture these hot electrons and generate reactive species by using visible-NIR light. The formation of metal-semiconductor heterojunctions allows hot electrons to be accepted into semiconductor conduction band and carry on the photocatalytic process (Figure 2a). The energetic barrier formed at the metal-semiconductor interface is called Schottky barrier [44]. Hot electrons are injected into semiconductor conduction band when their energy is superior to Schottky barrier energy (E_{SB}) which is lower than the bandgap of semiconductor (E_g) [45]. After the hot electron generation, holes are also generated in the plasmonic structure as illustrated in Figure 2b. For this mechanism to occur there must be a good interaction between the metal and the support, which make critical the synthesis step of these hybrid materials.

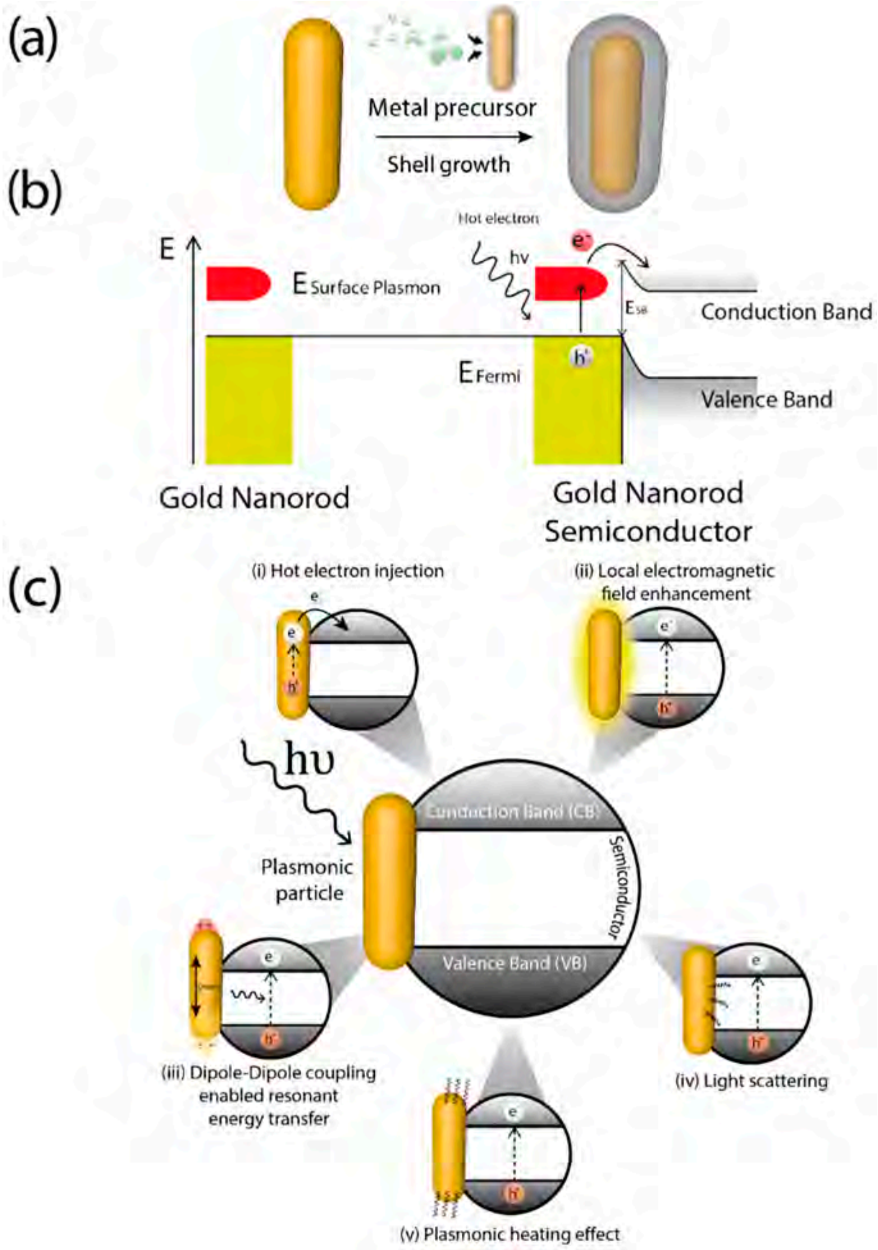

Figure 2. (**a**) Formation of Au-semiconductor heterostructures for the particular case of a core-shell structure. Different wet chemistry approaches are available to create a wide range of morphologies; (**b**) hot electron injection process. When a plasmonic structure as, in example, AuNR is irradiated with light with an energy equal to its LSPR, electrons mainly coming from conduction band are excited. If their energy overcomes the Schottky barrier energy (E_{SB}), they can be injected into the semiconductor conduction band to further perform the photocatalytic process; (**c**) mechanisms involved in plasmonic-semiconductor heterostructures (adapted from [46]). Diverse physical processes may take place between plasmonic nanostructure and semiconductor to promote valence band electrons to conduction band energy levels.

Nevertheless, several mechanisms could be involved independently or, most often, concurrently in photocatalysis using hybrid plasmonic materials [46]. Depending on the interaction of the plasmonic nanoparticle with the support and the electronic characteristic of the latter, plasmonic excitation can improve the photocatalytic properties of materials in several ways: (i) increasing absorption and scattering of light [47]; (ii) enhancing of the localized electric field [48]; (iii) hot charge carriers generation and transfer [49], already mentioned; (iv) dipole induction on non-polar molecules [50]; (v) local heat generation [46,51], depicted in Figure 2c.

Since nature, size, shape, and crystalline structure of the nanoparticle determine the energy of the LSPR [52] and in consequence the wavelength of the light used in photocatalysis, the control of those cited parameters is fundamental for the synthesis of suitable hybrid materials [53–55]. Concretely, the introduction of anisotropy in plasmonic-semiconductor systems adds a superior level of performance. Plasmonic Au cores exhibit a wide range of anisotropic nanostructures (nanoshells, nanorods, hollow spheres, nanoprisms, triangles, cubes, nanostars, urchins, etc.) with different LSPR [8,18,24,31,52,56] (Figure 3a). Typically, plasmon energy is concentrated on the sharpest edges of the anisotropic plasmonic nanostructures of high curvature [57–59] where light harvesting will take place more efficiently [60].

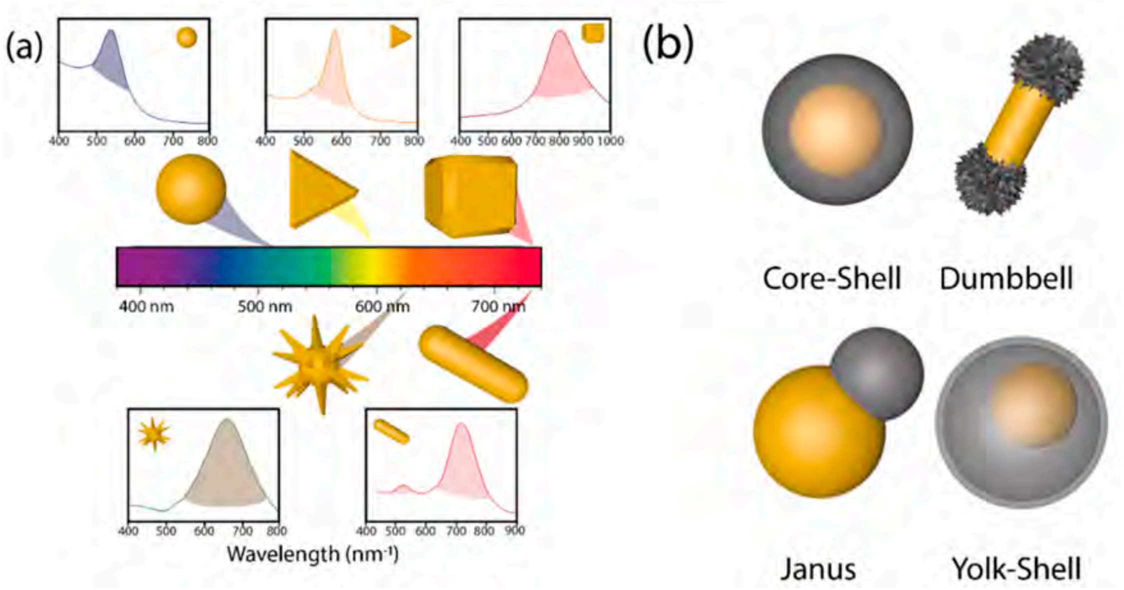

Figure 3. (**a**) The morphology of Au nanostructure determines LSPR shift. Au nanospheres, prisms, cages, urchin-like or rods exhibit different electron confinement, entailing different UV-vis. spectra; (**b**) Plasmonic-semiconductor heterostructures with different architectures, including core-shell (plasmonic nanoparticle as core and semiconductor as a surrounding shell), dumbbell (plasmonic AuNR where the semiconductor is selectively deposited on tips), Janus (plasmonic nanoparticle and semiconductor attached with both surfaces available for the substrates), and yolk-shell (plasmonic nanoparticle inside a voided semiconductor structure).

As shown in Figure 3b, it is possible to differentiate between core-shell, dumbbell, Janus, and yolk-shell configurations attending to the semiconductor distribution around the metallic cores [38] with several implications in their photocatalytic activity. Structures with exposed surfaces of both the metal and the semiconductors (i.e., dumbbell and Janus) exhibit a superior photocatalytic performance due to the continuous exposure of the reactants with the generated charge carriers (e^-/h^+) [27,40,60–64]. Different anisotropic heterostructures have been prepared with SiO_2 [65], Pt [66,67], Fe_2O_3 [68], Cu_2O [60], CeO_2 [63], and TiO_2 [27]. Yolk-shell structures (Figure 3b) are characterized by a hollow shell and an inner plasmonic core with several benefits for the photocatalytic process: (i) the presence of a hollow shell ensures higher specific surface area as it possesses an inner and external part. (ii) The small thickness of shells shortens charge diffusion distance, reducing possible bulk recombination processes, and (iii) void space present allows reflection of light inside the hollow shell, causing light scattering, and boosting the number of available photons [69].

3. Evaluation of Au-CeO_2 Anisotropic Hetero-Nanoarchitectures

The combination of plasmonic Au nanostructures with cerium oxide as complex hybrid architectures represents an interesting example of synergistic photocatalyst that maximizes the positive properties of each individual counterpart beyond the most explored TiO_2 or ZnO hybrids [70–72]. The redox properties of Ce endow this oxide with large capability to transport oxygen via Ce(IV)-Ce(III) pair redox cycles within its framework [21]. As a result, an extensive number of oxygen vacancies are present in ceria-based materials surface [73], favoring a continuous cycle of catalytic reaction-regeneration in oxidation reactions [21,74–77]. Nevertheless, CeO_2 exhibits two major drawbacks for photocatalytic purposes: (i) CeO_2 possesses a band gap of 3.2 eV burdening its photocatalytic response to the ultraviolet region; (ii) CeO_2 possesses low carrier mobility, hindering its transport to surface after the electron-hole pair photogeneration to react with the targeted substrates [78,79]·

Regarding the generation of the plasmonic hybrid photocatalyst, (i) CeO_2 as an n-type semiconductor possesses high density of states in its conduction band, which confers a good electron-accepting capability [40] and forms a heterojunction and Schottky barrier with Au to allow a proper hot-electron injection [21,22] (Figure 4). Therefore, the synthesis and development of Au-CeO_2 photocatalysts to maximize the redox properties of ceria has boosted the research on optimizing the interaction of these materials through an extended variety of imaginative configurations. Thus far, CeO_2 has been successfully deposited onto nanorods (both forming dumbbell [22] and core-shell [21,22,80] structures), spheres [21,81], or hollow cages [82].

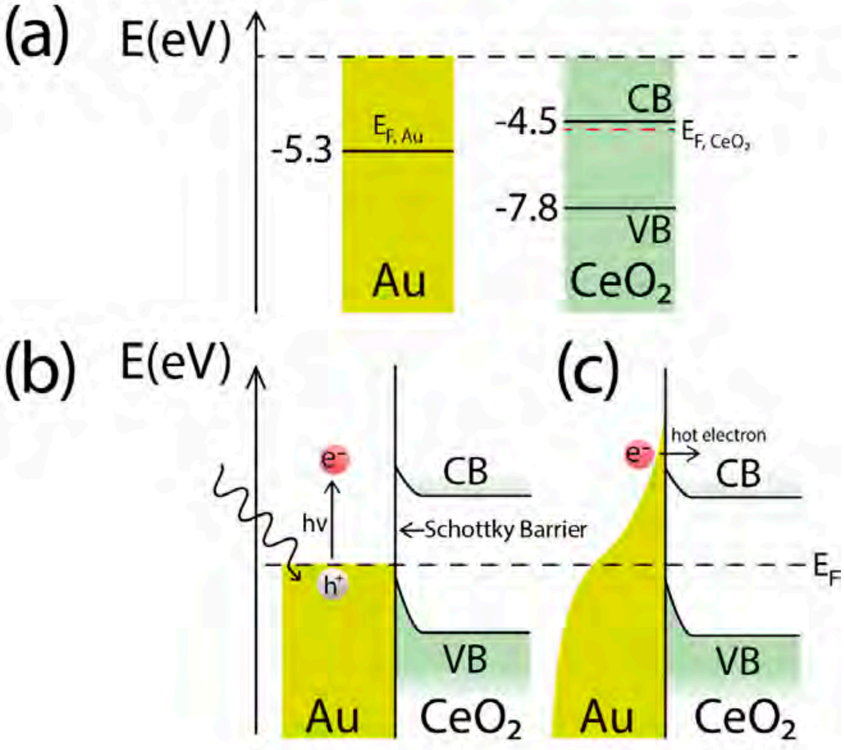

Figure 4. Energy band structure of Au-CeO_2 photocatalysts. (**a**) Energy band levels of Au and CeO_2 respectively; CeO_2 possess a relatively large band gap, needing from UV light to photo-generate charge carriers; (**b**) energy band distribution upon the gold plasmon excitation to (**c**) inject hot electrons into the conduction band of CeO_2.

In general, the synthesis of core-shell Au-CeO_2 nanostructures has been typically reported via hydrothermal treatment of a chelated Ce precursor [21,22,80–82]. Li et al. [21] reported the first synthesis of Au-CeO_2 nanostructures with core-shell configuration. One of the problems facing CeO_2 selective deposition on Au nanostructures was the rapid condensation of Ce precursors to form CeO_2. By using ethylenediaminetetraacetic acid (EDTA) as chelating agent, fast hydrolysis of Ce (III) ions could be prevented [83]. Thus, tuning Ce (III)/EDTA ratios allowed a fine control of CeO_2 deposition rates. Regarding the synthesis of dumbbell and Janus Au-CeO_2 systems, two outstanding contributions have been demonstrated in the recent literature by Pan et al. [63] and Jian et al. [22], respectively. It was possible to control the selective growth of CeO_2 on AuNR tips by controlling the amount of cetyltrimethylammonium bromide (CTABr) adsorbed onto the Au surface, which acted as a blockade of CeO_2 nucleation.

The first reported examples of Au-CeO_2 hybrids in photocatalysis were structurally analogous to the conventional counterparts traditionally used in heterogeneous catalysis for CO oxidation reactions. Kominaim et al. [84,85] reported the use of Au nanoparticles dispersed onto nanostructured CeO_2 supports to oxidize formic acid under visible light irradiation [84,85]. Nevertheless, Au-CeO_2 photocatalysts consisted in the random deposition of Au nanoparticles onto a relatively large CeO_2 support that prevented a deep understanding of the photocatalytic mechanism. As mentioned before, Li et al. [21] reported the first core-shell configuration for Au-CeO_2 nanoparticles. They tested the use of both spheres and rod-shaped Au plasmonic cores. The Au@CeO_2 catalysts exhibited different LSPR absorption maxima at different wavelengths within the visible-NIR region (530, 591, 715 nm, respectively) [21]. These hybrid configurations were employed towards the photooxidation of benzylic alcohol. The catalysts were subjected to calcination post-treatments to remove the excess of the directing surfactant employed to grow the ceria shell (CTABr), which did not possess any influence in the morphology/crystallinity of the sample. The influence of this calcination treatment was thoroughly evaluated upon irradiation with two different excitation sources (Xe lamp ($\lambda > 420$ nm) and laser ($\lambda = 671$ nm)). For Xe lamp, a systematic study of Au@$CeO_{2,\text{ LSPR 530nm}}$ was performed. It was found that the Au@CeO_2 calcined sample exhibited the highest photocatalytic activity, suggesting that the removal of CTABr enhanced the formation of Schottky barrier between Au and CeO_2 and facilitated a better charge carrier transfer in the catalyst. Upon laser irradiation, a similar trend was confirmed for the uncalcined and calcined samples, respectively. Calcined Au@$CeO_{2,\text{ LSPR 591nm}}$ showed the highest photocatalytic activity. The authors attributed the enhanced response to the better match between the LSPR absorption maximum of the calcined hybrid (redshifted after calcination to 680 nm) and the incident laser wavelength at 671 nm.

As previously pointed out in Figure 2c (vide supra), not only the hot electron injection pathway can supply electrons in the semiconductor conduction band. Interestingly, the generation of heat caused by one of the decay mechanisms caused by LSPR [86] can also promote the excitation of electrons from the valence band to the conduction band. As control experiments, Li et al. [21] studied the influence of the temperature in the catalytic activity in the absence of light. They found a considerable catalytic activity at the temperature that reached the system under illumination in darkness conditions, suggesting that part of the photocatalytic activity was thermally induced. As a potential mechanism (Figure 5a), the authors suggested a series of redox steps (vide infra): (i) electron injection into Ce(IV) conduction band, which generated Ce(III) species; (ii) O_2 adsorbed on previously generated Ce(III) sites forming Ce(IV)-O-O· (iii) that radical can remove α-H of benzyl alcohol yielding Ce(IV)-O-OH; (iv) the radical dehydrogenated benzylic alcohol combines with Ce(IV)-O-OH to produce the final benzaldehyde product and H_2O_2, and simultaneously, an electron returning to the Au bands to ensure electron-hole pair recombination.

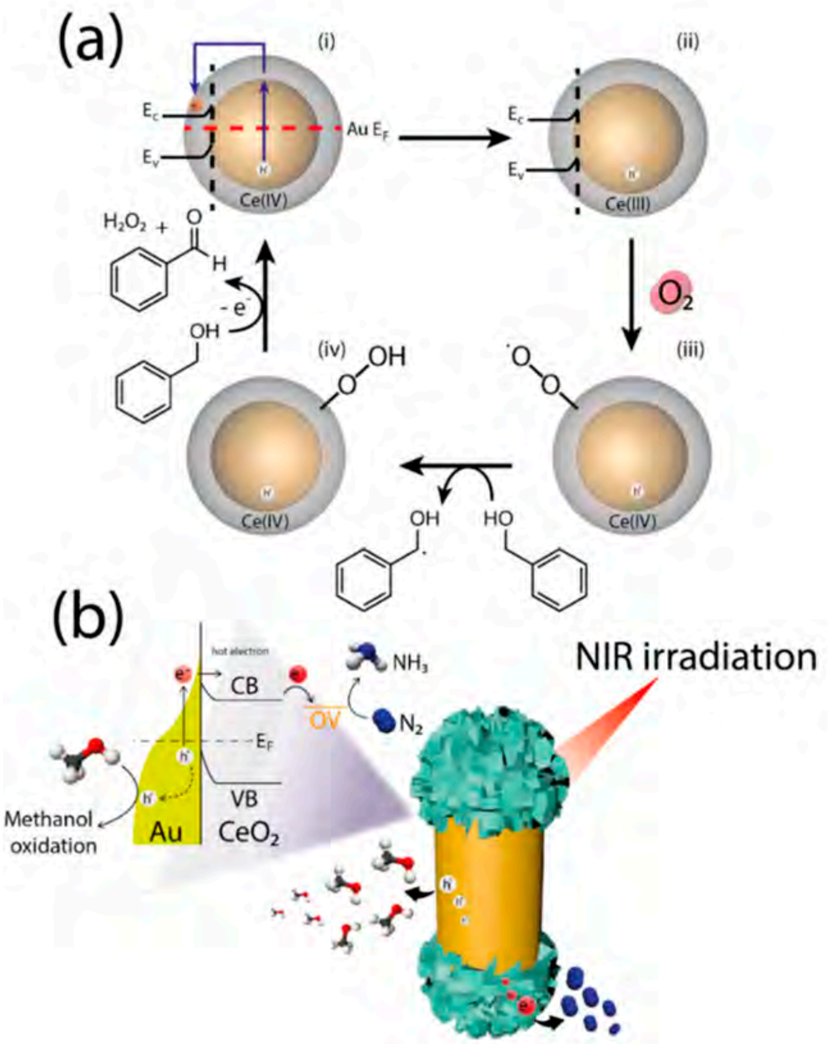

Figure 5. (**a**) Hot electron injection mechanism for a core-shell Au@CeO_2 configuration (adapted from [21]). Hot electrons generate Ce (III) species that can capture and activate O_2 which furtherly reacts with the substrate (benzylic alcohol). The generated Ce hydroperoxide (Ce-O-OH) reacts with the radical intermediate, yielding the final aldehyde; (**b**) photocatalytic mechanism for a dumbbell Au-CeO_2 structure (adapted from [22]). The generation and consumption (and thus, photocatalysis) of both hot electrons/holes is enhanced by promoting the accessibility of hole-acceptor molecules to the metallic surface and thanks to the accommodating role of oxygen vacancies (OVs) present in the ceria nanostructures. Core-shell architectures hinder this accessibility, accumulating hot holes and slowing down the catalytic cycle.

Alternatively, Wang et al. [80] demonstrated that the plasmon-induced hot-electron injection under NIR illumination in CeO_2 coated AuNRs with Janus configuration accelerated photo Fenton-like reactions using H_2O_2 as substrate. Again, the hot electron injection in Ce(IV) induced the formation of Ce(III) that acted as active species in Fenton-like reactions [87] with the generation of highly reactive ·OH that subsequently facilitated the degradation of an organic model pollutant. As depicted in Figure 5b, a heterostructure with plasmonic exposed faces possess important photocatalytic advantages. Pan et al. [63] demonstrated that half-encapsulated AuNRs with CeO_2 possessed better activity in the catalytic reduction of 4-nitrophenol (4-NP) with $NaBH_4$, in comparison with their core-shell AuNR@CeO_2 counterparts. Hot electrons were transferred from the plasmonic AuNR into CeO_2, generating holes on Au surface. BH_4 can donate electrons to AuNR generating H species that further convert 4-NP into 4-aminophenol. On the other hand, CeO_2 is able to withdraw e^- from AuNR that absorbs H^+ from H_2O yielding the same H active species [88]. This phenomenon could not occur in the case of core-shell AuNR@CeO_2 since Au facets remained unexposed to the liquid reaction media and yielded a lower catalytic activity.

Following a similar methodology, Jia et al. [22] combined CeO_2 with AuNRs forming a dumbbell heterostructure (Figure 5b) and evaluated their photocatalytic performance in the N_2 photofixation with NIR irradiation. CeO_2 rich surface in oxygen vacancies (OVs) (Ce(III) sites) chemisorbed N_2 that could be reduced to NH_3 by injected plasmonic hot electrons, breaking triple bond N-N. Due to the exposure of Au facets to the reaction media, as-generated hot holes could be consumed by a hole scavenger (in this particular case, methanol) to close the photocatalytic cycle. Core-shell AuNR@CeO_2 nanostructures prevented the availability of hot holes and the accessibility of CH_3OH to the active sites, which reflected in a huge difference in the NH_3 generation rate (114.3 vs. 18.44 $\mu mol \cdot h^{-1} \cdot g^{-1}$) [22]. Thus, CeO_2 emerges as a promising photocatalytic material in combination with Au plasmonic nanostructures, being the main highlights the regeneration of highly desired OVs due to hot electron transference from Au and the photothermo-induced oxygen mobility [21]. The high oxygen mobility has shown to have influence during the photothermo-catalytic process, as demonstrated by Li's experiments with temperature and in the absence of light [21,89]. CeO_2 as n-type semiconductor [90] and as oxygen ion conductor possess a unique charge separation effect: when a photon is absorbed, an electron is excited from the valence band (orbital O_{2p}) to an empty conduction band (orbital Ce_{4f}), forming a $Ce^{4+}(e^-)/O^{2-}$ (h^+) pair. The as-generated electrons remain localized in Ce (IV) centers favoring the charge separation and consequently, reducing the recombination phenomena (Figure 6) [90,91].

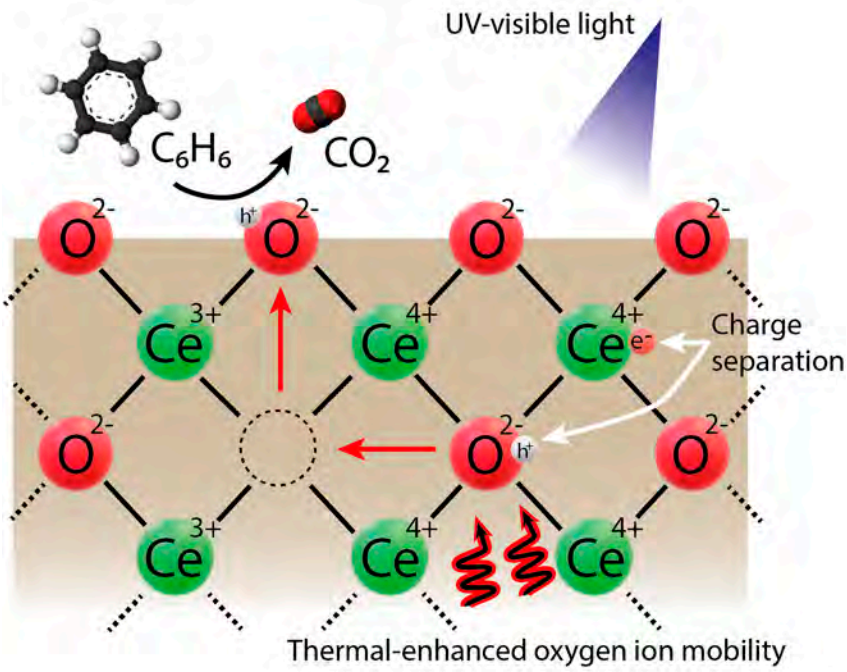

Figure 6. Schematic CeO_2 structure remarking the presence of OV and h^+/e^- separation. Plasmon-photothermal induced local heating in CeO_2 structure also enhances the oxygen ion mobility, facilitating the migration of $O^{2-}(h^+)$ species to the catalyst surface and, thus, enhancing the reaction (adapted from [89]).

Cited reports confirm an effective synergistic effect in the photocatalysis between LSPR and CeO_2 and an enhancement of the photocatalysis with Janus-type heterostructures [22,80]. Hence, synthetized Au-CeO_2 nanostructures interact with visible and NIR light, remarking the promising interest of these materials in environmental, biomedical applications and solar energy harvesting, among others [69,91–98].

4. Evaluation of Au-Cu_2O/Au-CuS Anisotropic Heteronanostructures

Cuprous oxide has attracted much attention as a photocatalyst due to its remarkable features as a semiconductor, and its extended variety of active roles in solar and energy applications of paramount interests for the Sustainable Development Goals targeted by most of the worldwide governments' agendas. Copper (I) oxide materials have been widely used in the degradation of organic compounds in solution and their photocatalytic activity has been studied against a large number of potential pollutants, such as organic material [99,100], drugs [101] or nutrients [102]. In addition, studies are also emerging where copper (I) oxide is being used in the generation of molecular hydrogen [32,103]. It is a highly abundant p-type semiconductor on earth with an energy band gap (E_g) of ≈ 2.17 eV that has a low cost and good absorption capabilities in the visible range when compared with other semiconductors [50,104]. However, some drawbacks have been also consistently reported for this oxide such as: (i) rapid recombination of electron-hole pairs; (ii) limited absorption of the semiconductor in the visible range; or (iii) natural tendency to form larger structures or disproportionation (especially in liquid media). The combination with anisotropic plasmonic cores to generate metal-semiconductor heterostructures represents an appealing alternative to overcome these problems [56,105,106]. These hybrid nanostructures offer two remarkable features, the Schottky barrier and the LSPR that improves the photocatalytic response by decreasing the carrier recombination rates and expanding the absorption range to the visible.

The selective growth of copper oxide onto plasmonic Au cores has been a trendy topic widely studied by multiple researchers in recent years [32,56,105–108]. However, the final morphology and selective exposure of specific crystalline facets has also attracted great interest in the field of photocatalysis in terms of both selectivity and reactivity [106,107,109]. The generation of core shell Au-Cu_2O hybrid structures with high precision has been reported in the recent literature [107,109,110]. Several parameters such as the nature of the reducing agents, the concentrations of reducing agent or pH values have been systematically evaluated to modulate the morphology, shape, and length of the oxide shells and favor the preferential exposure of selected crystal facets [32,109] (see Figure 7). For instance, Kuo et al. [109] reported the controlled synthesis of different morphologies including cubic structures, truncated cubes, cuboctahedra, or truncated octahedra to octahedra upon tuning the variation of NH_2OH. On the other hand, Kuo et al. [106] explored the influence of the different morphologies of AuNPs coated Cu_2O shell on the final photocatalytic performance towards the methyl orange (MO) degradation. They showed how core-shell architectures improved MO degradation from 18 to 50 $\mu mol \cdot cm^{-2}$ in comparison with pristine Cu_2O nanostructures and how the influence was higher in the case of the cube-shaped counterparts. This was an example where the plasmonic core helped in the transfer of carriers and promoted a better conductivity in a photo-electronic device. Yuan et al. [107] also developed hybrid AuNRs-copper oxide nanoparticles where they explored variations on the type of reducing agent to tune the preferential octahedral or cubo-octahedral morphologies (see Figure 7a). Both structures were generated by Ostwald ripening process. Smaller crystals were dissolved and redeposited onto larger crystals when different reductants were added. Hydrazine as stronger reductant was reported to promote the copper species to their more stable morphology. They also tested their photocatalytic activity towards the degradation of MO. It was observed how hybrid structures enhanced more activity in comparison with analogous bare semiconductor counterparts. The Au internal core performed in a dual way, LSPR promoted electron injection into the semiconductor and also acted as a charge sinker to increase charge migration and separation. This was a representative example on how the presence of the Au core considerably affects the activity of the system and how the morphology of the external shell (corner-truncated octahedral vs. regular octahedral Cu_2O) is also highly relevant in the absorption and degradation of MO. The truncated octahedral core-shell led to 94% MO conversion from an original 10 $mg \cdot L^{-1}$ MO concentration in 80 min [107]. This influence was also reported in Cu_2O nanoparticles with different morphologies that also exhibited a much higher photocatalytic activity in rhombohedral shaped structures due to the more selective MO absorption over <110> faces for subsequent further oxidation [111] (see Figure 7a). Recent studies have also reported the use of hollow Au cores to build Au-Cu_2O hybrids have also reported a successful tunability of their optical properties depending on their final architecture (Janus vs. core-shell). They reported an effective plasmon-induced energy transfer favored by the hollow Au nature that improved the MO degradation rates [56]. Other recent report by Xu et al. [112] has established a strong influence of the final heterostructure configuration on the capability to generate photocurrent. In this case, the used solid gold seeds incubated with a ligand that shifted the core-shell configuration towards a Janus-like structure.

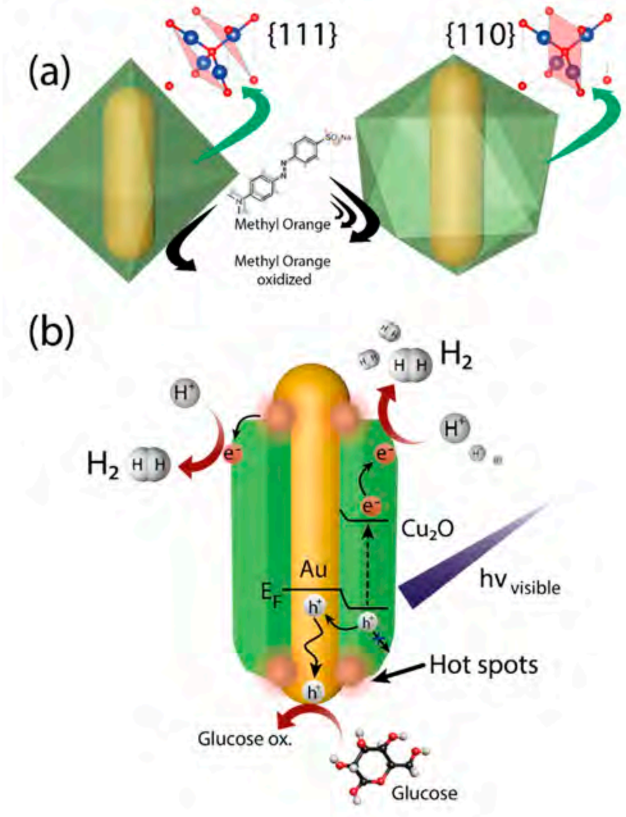

Figure 7. (**a**) Face dependent selectivity of Au@Cu_2O photoredox catalysis in MO degradation (adapted from [107]) (**b**) Selective Cu_2O deposition for partially/completely coated AuNR (adapted from [32]).

Additional studies have also exploited the synergy of Au- Cu_2O hybrid materials. For instance, Yu et al. developed [32] a hot-dog-like hybrid configuration where they selectively deposited copper oxide on the transverse part of large aspect ratio AuNRs, leaving the edges completely exposed [32]. It was possible to change the kind of Cu_2O-AuNR architecture from core-shell to tips-exposed hot-dog type structure by reducing the amount of copper precursor added to the synthesis. The preferential epitaxial growth of Cu_2O over the transversal part of AuNR promoted a first nucleation over these sides, leaving the edges completely uncoated under low copper concentration conditions. In a sequential manner, they even incorporated very thin TiO_2 layers on top of the copper oxide and established a critical evaluation of the photocatalytic activity for each hybrid configuration towards hydrogen production. The charge separation efficiency was significantly higher for the hot-dog configuration than for the bare Cu_2O or the fully-covered core-shell counterparts. The hot-dog configuration also exhibited an enhanced photocatalytic response almost 24-fold higher than the Cu_2O nanoparticles (80 μmol H_2 g^{-1} h^{-1} vs. 3.4 μmol H_2 g^{-1} h^{-1}) and four times higher than the core-shell configuration (19.3 μmol H_2 g^{-1} h^{-1}). The authors partially attributed the outperformance of the hot-dog configuration to the generation of four hot-spots at the interface of the non-coated AuNR and the semiconductor shells (see Figure 7b) of the hot-dog configuration. They concluded that this interface was more efficient in the transport of carriers due to the direct interaction of holes with glucose (used as sacrifice agent) and to the more efficient generation of hot electrons to induce the reduction step toward H_2 generation (see Figure 7b) [32]. The results were even better in the case of the ternary shell due to the more efficient p-n junction formed with the addition of a titania layer.

Even though ternary heterostructures are not the main focus of this review, it is worth mentioning recent efforts to build Z-schemed TiO_2-Au-Cu_2O photoelectrodes [30] or the addition of a third component of small Au NPs to the Au-Cu_2O hybrids reported by Yu et al. [113]. They designed a more complex core-shell AuNR@Cu_2O (octahedral) architecture additionally decorated with AuNPs (Figure 8). This ternary composite was able to increase the photocatalytic activity of the binary material by incorporating AuNPs, improving the transfer and separation of displaced charges through the semiconductor. Using higher wavelengths where Cu_2O is not able to absorb, light would penetrate through the structure reaching AuNR. Hot electrons could be generated via LSPR effect and injected into the conduction band of the semiconductor. Hot electrons and holes generated in the conduction band of Cu_2O could be promoted from bulk Cu_2O to the surface of the catalyst where the electrons are mainly trapped by Au nanoparticles to form singlet oxygen radical from the O_2 present on the surface. Meanwhile, holes places mainly in the surface of Cu_2O p-type semiconductor are used for the direct MO degradation. An electron transfer "push–pull" synergetic effect was enhanced with the help of both AuNR core and AuNPs on the surface of Cu_2O.

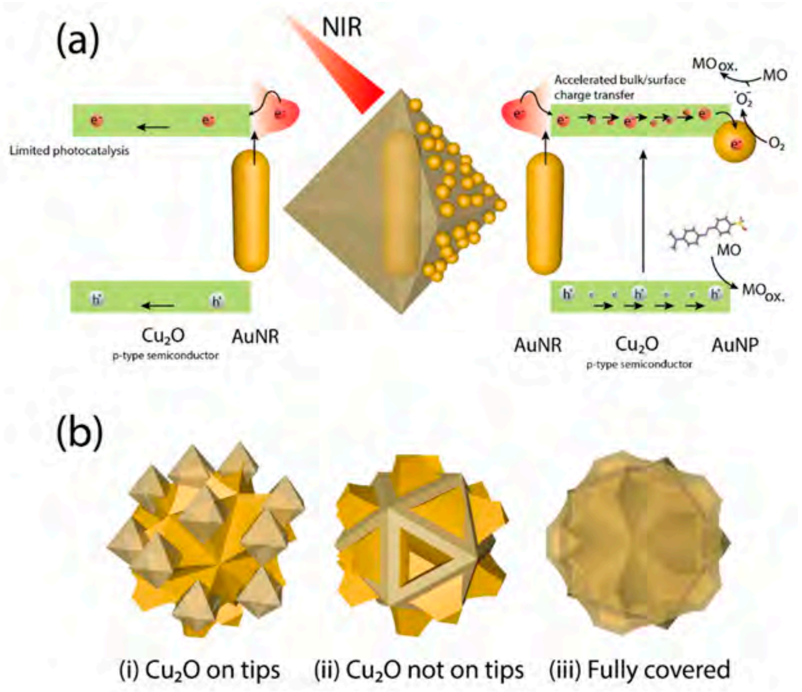

Figure 8. (**a**) Schematic mechanism for methyl orange (MO) photodegradation comparing the binary (left) from the ternary core-shell configuration (right) containing a plasmonic AuNR core, an octahedral Cu_2O shell and an additional layer of small AuNPs for the ternary alternative (adapted from [113]); (**b**) Selective Cu_2O deposition on AuNSs (adapted from [60]).

Sang Woo Han and co-workers conducted a comprehensive and systematic study where they developed hybrid plasmonic structures and explored how the variation of configuration affected the photocatalytic performance for hydrogen production using methanol as hole scavenger [60]. They synthesized plasmonic gold nanostars (Au NSs) and partially deposited copper monoxide (Cu_2O) tuning the stabilizing agent (sodium dodecyl sulfate (SDS), (CTABr), or Polyvinylpyrrolidone (PVP) (see Figure 8b). The Janus-like structures with <111> vertices completely covered by the semiconductor were achieved by using PVP as a stabilizing agent. A complete core-shell type configuration was achieved with the aid of sodium dodecyl sulfate (SDS) as a stabilizing agent and the structure with the exposed vertices was achieved by combining two surfactants, CTABr and SDS. The nature of each stabilizing agent was crucial for the selective deposition of the semiconductor (Cu_2O) onto the plasmonic Au NSs. Another important parameter to consider is the curvature of the surface of the plasmonic Au cores. In this systematic study, other Au seeds were used to prepare Janus-like architectures. It was observed how more shaped seeds could satisfactorily enhance the proposed architecture. However, it was not possible for less shaped seed structures using PVP as a stabilizing agent. In contrast, samples with less sharp vertex led to the preferential formation of core-shell type structures.

Yu et al. [60] also found that the use of PVP as a capping agent allowed a stronger interaction with low curvature sites from the Au NSs apexes, thereby leading to a preferential nucleation and growth of Cu_2O tips at those positions (see Figure 8b). Homogeneous core-shell heterostructures required the use of SDS instead of PVP. The random assembly and weaker protecting capability of SDS enabled a complete overgrowth of Cu_2O. In vertex-exposed Cu_2O-Au NSs a binary mixture of CTABr/SDS was used. The electrostatic interaction between both surfactants induced the generation of more stable micelles in aqueous solution that preferentially absorbed in the high-curvature sites, leaving the rest of Au nanostructure more accessible for Cu_2O nucleation. To further analyze the influence of the angle and the surfactants in the synthesis of anisotropic structures, AuNRs with different aspect ratios and binary mixtures of two surfactants (CTAB and SDS) were also evaluated by Yu and coworkers. They observed that the formation of Janus-type structures was preferentially induced as the aspect ratio of the AuNRs increased [60]. The authors studied the photocatalytic response of the different AuNSs-copper oxide configurations. A clear correlation between the efficiency of conversion of solar energy and the topology could be established during the hydrogen generation using methanol as sacrificing agent. Better conversions were achieved in partially covered structures compared to fully covered structures. Furthermore, no catalytic response was observed in the absence of the catalyst or in the presence of non-coated plasmonic cores. Furthermore, copper oxide of physical mixtures of both Cu_2O and AuNSs did not render any significant conversion, thereby reinforcing the synergistic role of the plasmonic photocatalyst with a well-defined architecture (especially for the Janus-type configurations).

The comparison of the photocatalytic activities among core shell-type structures with different plasmonic structures (spheres and stars) in their core can be explained considering the excitation capacity of both materials at different wavelengths. Using excitation wavelengths of 700/750 or 800 nm, the sharp surfaces of AuNSs caused a much higher plasmonic excitation than their spherical counterpart. Janus-like architectures present higher catalytic activity than Core-Shell structures. Not covered Au highly increased the final photocatalytic activity of hybrid structure letting the oxidation reaction of hole scavengers to occur for methanol, whereas core-shell architecture dramatically deprives the accessibility of Au surface to hole scavengers.

It is shown how using identical AuNSs cores with a Cu_2O overgrowth forming anisotropic heterostructures, induced completely different photocatalytic outcomes. It was observed a strong influence of Au-Cu_2O plasmon energy transfer. Coated vertex Au nanostar enhanced higher plasmon excitation in comparison to vertex exposed Au NSs configurations and leading the photocatalytic activity of hybrid structures under those experimental conditions [60]. To better understand the interaction mechanism between the plasmonic core and the outer semiconductor layer, the AuNSs were completely coated with a thin insulating SiO_2 layer prior to the subsequent deposition of copper oxide. The hybrids with the SiO_2 interlayer exhibited a considerable decrease in activity, pointing out that the mechanism of action was carried out by plasmon-induced photocatalysis [60].

Au-Cu_2O hybrid structures are being also currently explored for biomedical applications [114–117] such as photodynamic therapy treatment of cancer cells. Xu et al. [118] performed in vitro studies with AuCu-based materials, taking advantage of their ability to generate toxic reactive oxygen species (ROS) and its highly efficient phototherapy. AuNRs were used to selectively deposit copper on one of the sides of the Au structure using hexadecylamine as a protective ligand and sequentially making a coating with Au, which modified the structure inducing a galvanic replacement reaction and decreasing the amount of copper in the sample.

Interestingly, there are additional copper-based heterostructures where the semiconductor deposited over the plasmonic structure of Au is a Cu-based chalcogenide. These semiconductors are not expensive and more stable p-type semiconductors with a well-defined LSPR in the visible region. Furthermore, the amount of free charges in the material can be tuned upon modification of experimental parameters. Generating non-stoichiometric copper deficient structures of CuS induces the formation of transporters in the p-type semiconductor and exhibits subsequent properties such as photothermal catalysis or photocatalysis through the generation of ROS [119]. This type of structure can be made from previously formed copper oxides, giving rise to yolk shell-type structures where the plasmonic core was enclosed in an external copper chalcogenide shell and this can move freely within the voided structure [120]. To carry out the synthesis, it is typically necessary to obtain a copper (I) oxide structure through the conventional protocol, growing copper oxide following an epitaxial growth process. Later, the sample is sulfurized by introducing a sulfide precursor, such as Na_2S in an acidic medium, and it is allowed to evolve until the yolk-shell type structure is formed, maintaining the crystalline faces of the original Cu_2O structure. The catalytic ability of Au-CuS yolk shell structures to form ROS has been used in cancer chemotherapeutic therapies. Zhang et al. used the photothermal and photodynamic properties of this particular hybrid to perform a co-therapy using the resonance energy transfer (RET) mechanism [116].

Wang et al. [121] synthetized hybrid core-shell Au-CuS nanostructures directly without the need to use Cu_2O as a sacrificial agent in the formation of the nanostructure and modified the final properties of the photocatalyst through the non-stoichiometric growth of CuS at different amounts of copper. They carried out a systematic study in which they evaluated the photocatalytic properties at different wavelengths, ranging from UV to Infrared through the visible spectrum and determined the influence of the different parts of the hybrid nanoparticle on the activity of the catalysts. The plasmonic characteristics of the Au nucleus could be measured by changing its dimensions and modifying the thickness of the CuS coating deposited around it. On the other hand, the plasmonic characteristics of the copper sulfide shell could be modified by changing the concentration of free holes, which is closely linked with the crystalline phase of copper sulfide and the Cu:S ratios found.

Nanostructured Au can act as a photosensitizer (see Figure 2), being able to generate more electron-hole pairs in the semiconductor by means of RET mechanisms and thus improve the photocatalytic activity in the visible spectrum. Moreover, charge recombination in the surface of the semiconductor can be partially suppressed with the help of metals and charge migration through the bulk of Cu_2O could be enhance more easily in the presence of Au. The controlling deposition of copper around Au nanostructure enables an overall downsize of the hybrid nanoparticles compared with conventional Cu_2O nanostructures. It also allows a more selective deposition of Cu_2O. All these encountered possibilities appearing with hybrid structures have a positive influence to enhance the photocatalytic response of the hybrid.

5. Evaluation of Au-CdS Anisotropic Heteronanostructures

Other semiconductors commonly used in photocatalysis reactions are metal chalcogenides. However, some of their most remarkable features, such as the absorption of light at certain wavelengths or the separation of charges are far from optimal. For this reason, alternatives have been proposed to improve the photocatalytic properties of these systems when we use a range of wavelengths that encompasses the visible or infrared spectrum while achieving a better and more effective charge separation. An interesting alternative that arises from the need to solve this problem is to create hybrid metal-semiconductor nanostructures that allow the use of the visible-NIR spectrum thanks to the metal's plasmonic properties. Moreover, a wisely metal incorporation in semiconductor to form hybrid structure also improve the charge separation and its photocatalytic activity. Metal chalcogenides have been in the spotlight for the past years due to their versatility and potential number of applications in the energy field (i.e., photovoltaics, imaging). In addition, chalcogenides semiconductors have been also studied for photocatalytic emerging applications in solar energy conversion and renewable energy development [34,122–129].

Great interest has been devoted in recent years to the development of photocatalysts able to exploit the sun's energy to generate combustible, thus trying to reduce the amount of fossil fuels used [130,131]. One of the most interesting alternatives is H_2 generation as fuel using solar energy and semiconductor-based photocatalysts are postulated as one of the most promising alternatives to achieve this objective [132]. Some interesting features for solar-assisted photocatalysis in H_2 generation could be: [133] (i) It is necessary to find a semiconductor that has a narrow band gap and is highly efficient in absorption light; (ii) the band edge has to be more negative than standard hydrogen reduction potential; (iii) it should have good enough charge separation and migration to provide enough active sites.

There is a wide variety of photocatalysts but CdS is posited as a promising candidate for the generation of hydrogen. It has an optimal band gap of 2.4 eV that allows it to have photocatalytic activity under wavelengths of up to 500–600 nm in addition to a conduction band edge suitable for the generation of H_2 [134]. On the other hand, this semiconductor suffers from a rapid recombination of charges that make it inefficient. As an alternative to improve the migration and separation of charges, the generation of metal-semiconductor hybrids appears again as an alternative recently explored in the field [61,133–137]. In this particular hybrid, the rich existing chemistry of quantum dots has boosted the search for a wide variety of architectures searching the optimal coupling of energy levels necessary to improve the photocatalytic outcome towards H_2 production [34,136]. Developing anisotropic structures such as dumbbell type bimetallic particles [135,136], Janus-type particles [62], or yolk-shell structures [34,138] have reported considerable increases in the activity of the systems in comparison with more conventional core-shell type structures. No considerable activity enhancements have been shown in this latter configuration in comparison with the bare CdS semiconductor.

Zhao et al. [137], developed core-shell type hybrid structures and verified their efficiency in photocatalytic reactions for the production of hydrogen. They were able to synthesize concentric nanostructures where the plasmonic Au-core was completely covered by the semiconductor. Alternatively, they were also able to generate eccentric structures where the core of Au was shifted, having part of internal Au core exposed (see Figure 9a). For the synthesis of these nanostructures, a two-step multistage was necessary in which, first, silver-coated Au structures were generated in a core-shell configuration. Subsequently, the silver shell was sulfurized and a mixture of these nanoparticles were allowed to evolve with the cadmium precursor and certain conditions to enhance Au-CdS Janus-like/core shell-like nanoparticles. Zhao et al. reported [62] the need of eccentric nanoparticles of silver sulfide with partial crystallinity for further evolve into the generation of Janus-type structures. The catalytic studies showed that anisotropic materials with partially exposed Au core possessed much higher photocatalytic activity than completely coated core-shell configurations. A remarkable 730-fold enhancement in the H_2 evolution rates was detected for the anisotropic dimer (7.3 mmol H_2 $g^{-1}h^{-1}$ vs. 0.9 µmol H_2 $g^{-1}h^{-1}$, respectively). The authors claimed that increasing the temperature was necessary to ensure the proper presence of a well-defined crystalline phase. This phase was the niche that enabled a rational control of the anisotropy degree (see Figure 9a). In addition the partial exposure of the plasmonic Au was also determinant to maximize the SPR effects [62].

The photocatalytic activity of these hybrid structures was proved to have a highly symmetry dependence [137]. Janus-type particles were the most active, followed by analogous semiconductor particles and ending with core-shell Au-CdS nanoparticles. Furthermore, the Janus hybrids with the more pronounced anisotropy also exhibited the highest photoactivity using 300 W Xe lamp with application of a 400 nm cut-off long pass filter for water splitting reaction. This was attributed to the supporting role of Au acting as electron sink that could delay e/h^+ recombination rates and perform water reduction reaction. Upon excitation at wavelengths higher than 400 nm, a rapid electron transfer occurs between the conduction layers of the semiconductor (CdS) towards the Au surface thereby enabling a more efficient water reduction to generate hydrogen. However, the nanostructured bare

CdS or core-shell Au-CdS configurations prevent the separation of charges in such an efficient way and in the case of core-shell particles, the electrons remain trapped in the core of the particle and precluding the photocatalyst from an efficient hydrogen evolution reaction [137].

In an attempt to expand the photocatalytic response towards the less energetic NIR range and enhance core anisotropy, Li et al. [139] explored the possibilities of plasmonic AuNRs as inner plasmonic core. In this case, AuNRs were completely covered with silver to generate silver sulfide in a second step that would end up giving rise to CdS under certain conditions. Wang et al. [140] also developed more complex core shell-like nanostructures generating multilayered chalcogenide shells containing different combinations of Bi_2S_3 and CdS (Figure 9b,c). These samples were tested for dye photodegradation under visible region being the ternary combinations the most active in comparison with the binary counterparts (Au-Bi_2S_3 or Au-CdS). The enhancement observed in the ternary component was attributed to the transfer of electrons from the exposed semiconductor (CdS) with a 2.4 eV band gap passing through the Bi_2S_3 semiconductor intermediate layer with a 1.32 eV band gap until reaching the internal Au core. However, holes as positive charges, take longer to move from the valence layer from one semiconductor to another, enabling charges separation and, therefore, increasing photocatalytic activity. Moreover, hot electron injection from visible activated dumbbell-like AuNR to semiconductor can considerably increase the photoactivity compared with bare semiconductor or semiconductor coated conventional GNRs (see Figure 9b,c).

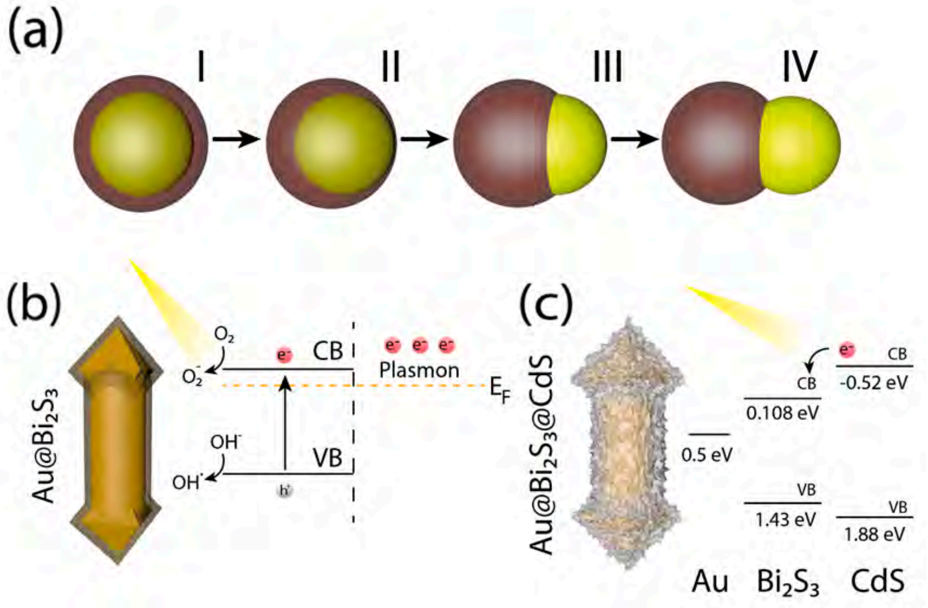

Figure 9. (**a**) Concentric core-shell (I), eccentric core-shell (II), and Janus (III, IV) hybrid structures (adapted from [137]); (**b**) AuNR@Bi_2S_3 hybrid structure and its excitation mechanism under visible light irradiation; (**c**) AuNR@Bi_2S_3@CdS core-(double) shell hybrid structure. Excitation mechanism for a more efficient carrier migration and its considerable improvement when both semiconductors were coupled in a double shell structure (adapted from [140]).

Xu et al. [136] developed different metal-CdS hybrid bimetallic structures and evaluated their photocatalytic activity to form benzaldehyde and H_2. They synthesized three types of plasmonic heteronanostructures: CdS coated AuNRs, CdS coated-Pt coated AuNRs, and CdS coated-Pt tipped AuNRs and compared their photocatalytic activity. It was observed an increasing order of activity: Au@CdS < Au@Pt@CdS < Au-Pt@CdS (50 vs. 100 vs. 150 μmol H_2 g^{-1} h^{-1}, respectively). They also carried out controls with the CdS semiconductor and metallic nanoparticles, but the activity decreased considerably in both cases. In this study, the use of AuNRs improved the harvesting of visible-NIR light and induces a local electric field (Figure 2) that is capable of promoting the generation and separation of charges from the CdS semiconductor (Figure 10). The anisotropically deposited platinum at the edge of the nanorod acted as an electron sinker or electron reservoir enabling the electrons to be directed to the places where the reduction reaction of the protons takes place to obtain H_2. In addition, the asymmetric separation of both metals served as a highway for an efficient transport of electrons that partially prevent electron-hole recombination (see Figure 10). This represents another good example of how smart designs and proper understanding of the carrier transport mechanisms facilitates an improved photo-response outperforming the simpler configurations.

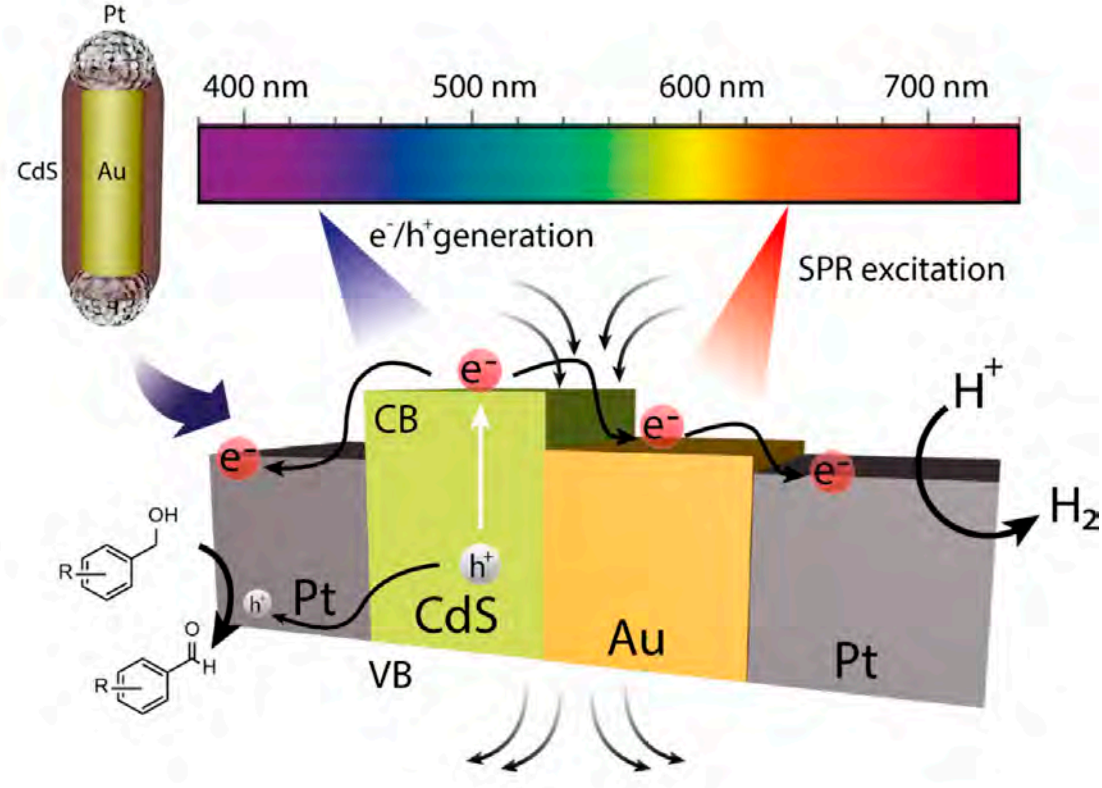

Figure 10. Schematic representation of the energy band multichannel in bimetallic@CdS heterostructures (adapted from [136]); semiconductor charge separation under visible light irradiation and its further electron migration through AuNRs to enhance tipped Pt reservoir; Induced both the resonance energy transfer (RET) and hot electron transfer processes and synergistically boosted the photocatalytic reaction (adapted from [136]).

Wu et al. [135] explored an analogous combination of Au-Pt-CdS components structured in core-shell (Au@CdS) or AuPt-CdS dumbbell like configurations with different coverage degree (see Figure 11a). These hybrids were systematically tested in the photocatalytic hydrogen generation reaction under visible or NIR light irradiation [135]. The photocatalytic activities were compared when systems were faced with wavelengths belonging to the visible or the near infrared light and it was seen that the order in the activity depended not only on the type of structure used, but also on the wavelength used because of the mechanisms enhancement. When the catalysts were excited with wavelengths within the visible range, the order in the catalytic activity was as follows: Au-Pt-CdS >> Au@CdS > CdS >> Au-Pt. In contrast, when NIR illumination was used, the activity dropped significantly, and the order of the catalytic activity was: Au-Pt > Au-Pt@CdS > Au > Au@CdS. Still, the H_2 evolution rates (in the micromolar range) were less remarkable than those reported for the heterodimers (vide supra).

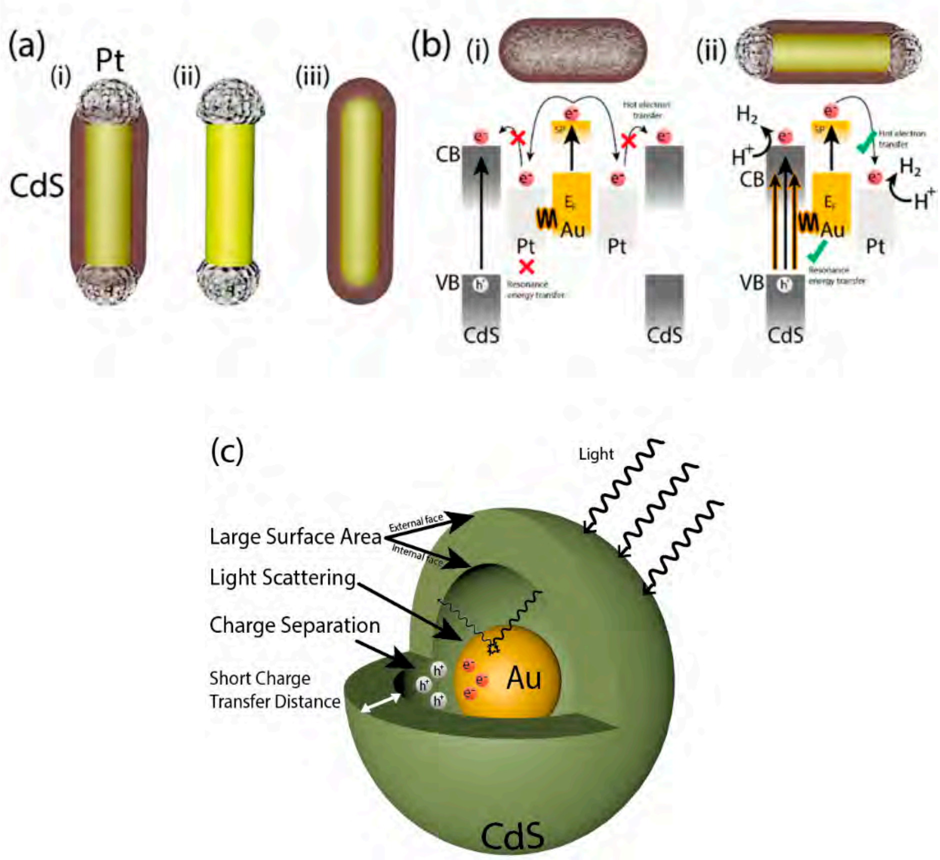

Figure 11. (**a**) Representation of Au-Pt@CdS (i), Au-Pt (ii), Au@CdS (iii) anisotropic hybrid structures; (**b**) schematic representation of energy band multichannel of Au@CdS and Au-Pt@CdS (adapted from [135]) and comparative excitation pathways: Au-assisted CdS charge separation and Au-Pt hot electron transfer is enhanced in the anisotropic structure. Hot electron transfer or RET is not easily achieved when Pt shell is deposited over AuNRs (adapted from [135]); (**c**) schematic representation of photoactivation mechanisms in yolk-shell Au-CdS nanostructures (adapted from [138]).

Under sunlight illumination, CdS semiconductor deposited on the sides of Pt-Au bimetallic nanoparticle induced both the RET and hot electron transfer processes and synergistically boosted the photocatalytic H_2 generation. However, when catalysts were activated by infrared light, Au-Pt bimetallic structure became the most active architecture indicating that excited hot electrons can further transfer to tipped Pt, but it is more complicated for electrons to enhance further migration from AuNR to CdS semiconductor (see mechanisms in Figure 11b). It was also observed how the catalytic activity of CdS coated metal tipped AuNRs (Au-Pt-CdS) was more active than its concentric counterpart Au@Pt@Cds when nanocatalyst were activated with visible light. The transversal LSPR induced electric field cannot reach the outside CdS semiconductor due to the presence of Pt NPs between the inner Au core and the external CdS layer (see Figure 11b). Pt nanoparticles around AuNR prevented the charge transfer between CdS and Au internal core. It has been observed how strategically modulating the metallic core of the structure by incorporating anisotropy or integrating several metals in a controlled way, the activity of the system was highly increased.

Likewise, yolk-shell structures have been recently reported as promising alternative hybrids with enhanced photocatalytic outcome provided by the selective control of the shell properties [138,141]. Han et al. [138] developed yolk-shell structures containing a plasmonic AuNR. The photocatalytic activity towards the generation of H_2 was compared to analogous core-shell type architectures and hollow CdS nanoparticles [138]. Using hole scavengers such as Na_2S or Na_2SO_3 to avoid photocorrosion of the CdS and exciting upon visible wavelengths, the yolk-shell structure generated a hydrogen conversion over 27 (1.7 mmol H_2 $g^{-1}h^{-1}$) or 12 (0.5 mmol H_2 $g^{-1}h^{-1}$) times greater than the core-shell type and hollow semiconductor structures (0.02 mmol H_2 $g^{-1}h^{-1}$). The authors also compared the catalytic activity of the yolk-shell Au-CdS hybrid system with an analogous system containing an insulating intermediate layer of silicon oxide Au@SiO_2-CdS [138]. No significant differences were observed when compared both photocatalysts under the same experimental conditions. For further explanation, several mechanisms were proposed.

The thermal activity of the rod was tentatively considered as one of the possible causes of the increase in activity, but the thermal evolution of the system for all photocatalysts was very similar. Since higher activity was achieved by using Au-coated plasmonic structures covered with SiO_2, it was concluded that plasmon energy transfer or plasmon-induced RET (see Figure 10) was not the mechanism by which these systems increased their activity. The researchers determined that the main cause for this process was radiative relaxation of the SPR of the AuNRs, such as near-field enhancement and resonant photon scattering (see Figures 2 and 11c). More recent studies have concurred in finding higher activity for the yolk-shell type [34]. Yolk-shell type structures have the ability to generate a very large surface-to-volume ratio, increasing the amount of surface exposed for photocatalysis and decreasing the amount of bulk material to reduce charge recombination probabilities. In addition, plasmonic Au is capable of generating better charge separation as well as potential light scattering of the light inside the nanoparticle (see Figure 11c).

We have seen several examples of hybrid architectures, where not only the type of metal incorporated (Au, Pt) was important, but its arrangement with respect to the CdS semiconductor played a crucial role in enhancing the catalytic activity. Yolk-shell type structures provided a better optical response thanks to the light scattering generated in the internal part of this void structure. Dumbbell-like Au-Pt type bimetallic structures allow better migration and separation of charges, solving one of the most important problems of this type of semiconductor. It is important to highlight the development of CdS-based complex hybrid structures where a good design and configuration of the constructed architecture allows us to considerably improve the activity of these systems when it is compared with other less complex hybrid structures, such as bare CdS or core-shell architectures.

6. Conclusions

TiO_2 and ZnO assembled with plasmonic metals are still the most explored and developed heteronanostructures obtained using semiconductors. The search for novel alternatives that can expand and take advantage of the full-solar irradiation spectra has stimulated the search for novel alternatives that can provide additional features in terms of more efficient harvesting properties, more effective carrier transport and enhanced selectivities towards specific end-products. In this regard, the need to find newer and cleaner routes for energy production, the need to improve the efficiency of decontamination of harmful pollutants and the willingness to promote the revalorization of wastes or unwanted byproducts has boosted the research in the area of photocatalysis. Nowadays, the innovation in the design of smart combination of metal-semiconductors continue to be a very promising alternative. In this review, we presented some of the most promising and versatile alternative gold-semiconductor heterostructures. The main results highlighted throughout this revision of the most recent literature suggests an important morphology dependence in the final outcome and how less-conventional designs beyond core-shell configurations may pave the way for important breakthroughs in forthcoming years. Furthermore, the selection of anisotropic metals also represents an appealing strategy to maximize the virtues of plasmon excitation. Finally, we would like to make emphasis on the need to establish exquisite control and definition of these hetero-nanoarchitectures at the nanoscale level in order to establish a clear progress in biomedical applications, where size control and reproducibility are key for clinical translation.

Author Contributions: Conceptualization, J.L.H.; writing—original draft preparation, J.I.G.-P., J.B.-A., C.J.B.-A., J.L.H.; writing—review and editing, J.L.H. All authors have read and agreed to the published version of the manuscript.

Funding: This research was funded by the European Research Council (ERC) through an Advanced Research Grant (CADENCE, grant number 742684). The APC was waived by the journal.

Acknowledgments: The authors thank the Platform of Production of Biomaterials and Nanoparticles of the NANBIOSIS-ICTS of the CIBER in BioEngineering, Biomaterials & Nanomedicine (CIBER-BBN). J.B.-A. acknowledges the Spanish Government for a PhD predoctoral grant (FPU18/04618). J.I.G.-P. thanks the Regional Government of Aragon (DGA) for granting a PhD predoctoral contract. The Regional Government of Aragon is also acknowledged.

Conflicts of Interest: The authors declare no conflict of interest.

References

1. Eibner, A.J.C.-Z. Action of light on pigments I. *Chem-Ztg* **1911**, *35*, 753–755.
2. Coronado, J.M. A historical introduction to photocatalysis. In *Design of Advanced Photocatalytic Materials for Energy and Environmental Applications*; Coronado, J.M., Fresno, F., Hernández-Alonso, M.D., Portela, R., Eds.; Springer: London, UK, 2013; pp. 1–4. [CrossRef]
3. Reyes-Coronado, D.; Rodríguez-Gattorno, G.; Espinosa-Pesqueira, M.E.; Cab, C.; de Coss, R.; Oskam, G. Phase-pure TiO2nanoparticles: Anatase, brookite and rutile. *Nanotechnology* **2008**, *19*, 145605. [CrossRef] [PubMed]
4. Bakin, A.; El-Shaer, A.; Mofor, A.C.; Al-Suleiman, M.; Schlenker, E.; Waag, A. ZnMgO-ZnO quantum wells embedded in ZnO nanopillars: Towards realisation of nano-LEDs. *Phys. Status Solidi C* **2007**, *4*, 158–161. [CrossRef]
5. Bueno-Alejo, C.J.; Graus, J.; Arenal, R.; Lafuente, M.; Bottega-Pergher, B.; Hueso, J.L. Anisotropic Au-ZnO photocatalyst for the visible-light expanded oxidation of n-hexane. *Catal. Today* **2020**. [CrossRef]
6. Ortega-Liebana, M.C.; Hueso, J.L.; Ferdousi, S.; Arenal, R.; Irusta, S.; Yeung, K.L.; Santamaria, J. Extraordinary sensitizing effect of co-doped carbon nanodots derived from mate herb: Application to enhanced photocatalytic degradation of chlorinated wastewater compounds under visible light. *Appl. Catal. B Environ.* **2017**, *218*, 68–79. [CrossRef]
7. Suarez, H.; Ramirez, A.; Bueno-Alejo, C.J.; Hueso, J.L. Silver-copper oxide heteronanostructures for the plasmonic-enhanced photocatalytic oxidation of N-hexane in the visible-NIR range. *Materials* **2019**, *12*, 3858. [CrossRef]
8. Graus, J.; Bueno-Alejo, C.J.; Hueso, J.L. In-situ deposition of plasmonic gold nanotriangles and nanoprisms onto layered hydroxides for full-range photocatalytic response towards the selective reduction of p-nitrophenol. *Catalysts* **2018**, *8*, 354. [CrossRef]
9. Mas, N.; Hueso, J.L.; Martinez, G.; Madrid, A.; Mallada, R.; Ortega-Liebana, M.C.; Bueno-Alejo, C.; Santamaria, J. Laser-driven direct synthesis of carbon nanodots and application as sensitizers for visible-light photocatalysis. *Carbon* **2020**, *156*, 453–462. [CrossRef]
10. Kawamura, G.; Matsuda, A. Synthesis of plasmonic photocatalysts for water splitting. *Catalysts* **2019**, *9*, 982. [CrossRef]
11. Wang, J.; Wang, X.; Mu, X. Plasmonic photocatalysts monitored by tip-enhanced raman spectroscopy. *Catalysts* **2019**, *9*, 109. [CrossRef]
12. Gong, Z.; Ji, J.; Wang, J. Photocatalytic reversible reactions driven by localized surface plasmon resonance. *Catalysts* **2019**, *9*, 193. [CrossRef]
13. Wei, Z.; Janczarek, M.; Wang, K.; Zheng, S.; Kowalska, E. Morphology-governed performance of plasmonic photocatalysts. *Catalysts* **2020**, *10*, 1070. [CrossRef]
14. Fang, J.; Cao, S.-W.; Wang, Z.; Shahjamali, M.M.; Loo, S.C.J.; Barber, J.; Xue, C. Mesoporous plasmonic Au–TiO2 nanocomposites for efficient visible-light-driven photocatalytic water reduction. *Int. J. Hydrogen Energy* **2012**, *37*, 17853–17861. [CrossRef]
15. Fragua, D.M.; Abargues, R.; Rodriguez-Canto, P.J.; Sanchez-Royo, J.F.; Agouram, S.; Martinez-Pastor, J.P. Au–ZnO nanocomposite films for plasmonic photocatalysis. *Adv. Mater. Interfaces* **2015**, *2*, 1500156. [CrossRef]

16. Kim, M.; Lin, M.; Son, J.; Xu, H.; Nam, J.-M. Hot-electron-mediated photochemical reactions: Principles, recent advances, and challenges. *Adv. Opt. Mater.* **2017**, *5*, 1700004. [CrossRef]
17. Liu, J.; Ma, N.; Wu, W.; He, Q. Recent progress on photocatalytic heterostructures with full solar spectral responses. *Chem. Eng. J.* **2020**, *393*, 124719. [CrossRef]
18. Volokh, M.; Mokari, T. Metal/semiconductor interfaces in nanoscale objects: Synthesis, emerging properties and applications of hybrid nanostructures. *Nanoscale Adv.* **2020**, *2*, 930–961. [CrossRef]
19. Ghosh Chaudhuri, R.; Paria, S. Core/Shell nanoparticles: Classes, properties, synthesis mechanisms, characterization, and applications. *Chem. Rev.* **2012**, *112*, 2373–2433. [CrossRef] [PubMed]
20. Dutta, S.K.; Mehetor, S.K.; Pradhan, N. Metal semiconductor heterostructures for photocatalytic conversion of light energy. *J. Phys. Chem. Lett.* **2015**, *6*, 936–944. [CrossRef]
21. Li, B.; Gu, T.; Ming, T.; Wang, J.; Wang, P.; Wang, J.; Yu, J.C. (Gold Core)@(Ceria Shell) nanostructures for plasmon-enhanced catalytic reactions under visible light. *ACS Nano* **2014**, *8*, 8152–8162. [CrossRef]
22. Jia, H.; Du, A.; Zhang, H.; Yang, J.; Jiang, R.; Wang, J.; Zhang, C.-Y. Site-selective growth of crystalline ceria with oxygen vacancies on gold nanocrystals for near-infrared nitrogen photofixation. *J. Am. Chem. Soc.* **2019**, *141*, 5083–5086. [CrossRef] [PubMed]
23. Chen, T.-M.; Xu, G.-Y.; Ren, H.; Zhang, H.; Tian, Z.-Q.; Li, J.-F. Synthesis of Au@TiO2 core–shell nanoparticles with tunable structures for plasmon-enhanced photocatalysis. *Nanoscale Adv.* **2019**, *1*, 4522–4528. [CrossRef]
24. Liu, T.-M.; Conde, J.; Lipiński, T.; Bednarkiewicz, A.; Huang, C.-C. Revisiting the classification of NIR-absorbing/emitting nanomaterials for in vivo bioapplications. *NPG Asia Mater.* **2016**, *8*, e295. [CrossRef]
25. Ola, O.; Maroto-Valer, M.M. Review of material design and reactor engineering on TiO_2 photocatalysis for CO_2 reduction. *J. Photochem. Photobiol. C Photochem. Rev.* **2015**, *24*, 16–42. [CrossRef]
26. Habisreutinger, S.N.; Schmidt-Mende, L.; Stolarczyk, J.K. Photocatalytic reduction of CO_2 on TiO_2 and other semiconductors. *Angew. Chem. Int. Ed.* **2013**, *52*, 7372–7408. [CrossRef] [PubMed]
27. Wu, B.; Liu, D.; Mubeen, S.; Chuong, T.T.; Moskovits, M.; Stucky, G.D. Anisotropic growth of TiO_2 onto gold nanorods for plasmon-enhanced hydrogen production from water reduction. *J. Am. Chem. Soc.* **2016**, *138*, 1114–1117. [CrossRef] [PubMed]
28. Seh, Z.W.; Liu, S.; Low, M.; Zhang, S.Y.; Liu, Z.; Mlayah, A.; Han, M.Y. Janus Au-TiO_2 photocatalysts with strong localization of plasmonic near-fields for efficient visible-light hydrogen generation. *Adv. Mater. (Deerfield Beach Fla.)* **2012**, *24*, 2310–2314. [CrossRef]
29. Sun, H.; He, Q.; Zeng, S.; She, P.; Zhang, X.; Li, J.; Liu, Z. Controllable growth of Au@TiO2 yolk–shell nanoparticles and their geometry parameter effects on photocatalytic activity. *New J. Chem.* **2017**, *41*, 7244–7252. [CrossRef]
30. Li, J.-M.; Tsao, C.-W.; Fang, M.-J.; Chen, C.-C.; Liu, C.-W.; Hsu, Y.-J. TiO2-Au-Cu2O photocathodes: Au-mediated z-scheme charge transfer for efficient solar-driven photoelectrochemical reduction. *ACS Appl. Nano Mater.* **2018**, *1*, 6843–6853. [CrossRef]
31. Han, C.; Qi, M.-Y.; Tang, Z.-R.; Gong, J.; Xu, Y.-J. Gold nanorods-based hybrids with tailored structures for photoredox catalysis: Fundamental science, materials design and applications. *Nano Today* **2019**, *27*, 48–72. [CrossRef]
32. Yu, X.; Liu, F.; Bi, J.; Wang, B.; Yang, S. Improving the plasmonic efficiency of the Au nanorod-semiconductor photocatalysis toward water reduction by constructing a unique hot-dog nanostructure. *Nano Energy* **2017**, *33*, 469–475. [CrossRef]
33. Zhu, M.; Wang, Y.; Deng, Y.-H.; Peng, X.; Wang, X.; Yuan, H.; Yang, Z.-J.; Wang, Y.; Wang, H. Strategic modulation of energy transfer in Au-TiO_2-Pt nanodumbbells: Plasmon-enhanced hydrogen evolution reaction. *Nanoscale* **2020**, *12*, 7035–7044. [CrossRef] [PubMed]
34. Wang, L.; Chong, J.; Fu, Y.; Li, R.; Liu, J.; Huang, M. A novel strategy for the design of Au@CdS yolk-shell nanostructures and their photocatalytic properties. *J. Alloys Compd.* **2020**, *834*, 155051. [CrossRef]
35. Atta, S.; Pennington, A.M.; Celik, F.E.; Fabris, L. TiO_2 on Gold Nanostars Enhances Photocatalytic Water Reduction in the Near-Infrared Regime. *Chem* **2018**, *4*, 2140–2153. [CrossRef]
36. Sun, Y.; Sun, Y.; Zhang, T.; Chen, G.; Zhang, F.; Liu, D.; Cai, W.; Li, Y.; Yang, X.; Li, C. Complete Au@ZnO core–shell nanoparticles with enhanced plasmonic absorption enabling significantly improved photocatalysis. *Nanoscale* **2016**, *8*, 10774–10782. [CrossRef] [PubMed]

37. Shao, X.; Li, B.; Zhang, B.; Shao, L.; Wu, Y. Au@ZnO core–shell nanostructures with plasmon-induced visible-light photocatalytic and photoelectrochemical properties. *Inorg. Chem. Front.* **2016**, *3*, 934–943. [CrossRef]
38. Jiang, R.; Li, B.; Fang, C.; Wang, J. Metal/Semiconductor hybrid nanostructures for plasmon-enhanced applications. *Adv. Mater.* **2014**, *26*, 5274–5309. [CrossRef]
39. Zhou, N.; López-Puente, V.; Wang, Q.; Polavarapu, L.; Pastoriza-Santos, I.; Xu, Q.-H. Plasmon-enhanced light harvesting: Applications in enhanced photocatalysis, photodynamic therapy and photovoltaics. *RSC Adv.* **2015**, *5*, 29076–29097. [CrossRef]
40. Clavero, C. Plasmon-induced hot-electron generation at nanoparticle/metal-oxide interfaces for photovoltaic and photocatalytic devices. *Nat. Photonics* **2014**, *8*, 95–103. [CrossRef]
41. Semenov, A.D.; Gol tsman, G.N.; Sobolewski, R. Hot-electron effect in superconductors and its applications for radiation sensors. *Supercond. Sci. Technol.* **2002**, *15*, R1–R16. [CrossRef]
42. Knight, M.W.; Wang, Y.; Urban, A.S.; Sobhani, A.; Zheng, B.Y.; Nordlander, P.; Halas, N.J. Embedding plasmonic nanostructure diodes enhances hot electron emission. *Nano Lett.* **2013**, *13*, 1687–1692. [CrossRef] [PubMed]
43. White, T.P.; Catchpole, K.R. Plasmon-enhanced internal photoemission for photovoltaics: Theoretical efficiency limits. *Appl. Phys. Lett.* **2012**, *101*, 073905. [CrossRef]
44. Tung, R.T. The physics and chemistry of the Schottky barrier height. *Appl. Phys. Rev.* **2014**, *1*, 011304. [CrossRef]
45. Knight, M.W.; Sobhani, H.; Nordlander, P.; Halas, N.J. Photodetection with active optical antennas. *Science* **2011**, *332*, 702. [CrossRef] [PubMed]
46. Zhang, N.; Han, C.; Fu, X.; Xu, Y.-J. Function-oriented engineering of metal-based nanohybrids for photoredox catalysis: Exerting plasmonic effect and beyond. *Chem* **2018**, *4*, 1832–1861. [CrossRef]
47. Kochuveedu, S.T.; Jang, Y.H.; Kim, D.H. A study on the mechanism for the interaction of light with noble metal-metal oxide semiconductor nanostructures for various photophysical applications. *Chem. Soc. Rev.* **2013**, *42*, 8467–8493. [CrossRef]
48. Liu, Z.; Hou, W.; Pavaskar, P.; Aykol, M.; Cronin, S.B. Plasmon resonant enhancement of photocatalytic water splitting under visible illumination. *Nano Lett.* **2011**, *11*, 1111–1116. [CrossRef]
49. Tian, Y.; Tatsuma, T. Plasmon-induced photoelectrochemistry at metal nanoparticles supported on nanoporous TiO_2. *Chem. Commun.* **2004**, 1810–1811. [CrossRef]
50. Cushing, S.K.; Li, J.; Meng, F.; Senty, T.R.; Suri, S.; Zhi, M.; Li, M.; Bristow, A.D.; Wu, N. Photocatalytic activity enhanced by plasmonic resonant energy transfer from metal to semiconductor. *J. Am. Chem. Soc.* **2012**, *134*, 15033–15041. [CrossRef]
51. Christopher, P.; Ingram, D.B.; Linic, S. Enhancing photochemical activity of semiconductor nanoparticles with optically active Ag nanostructures: Photochemistry mediated by ag surface plasmons. *J. Phys. Chem. C* **2010**, *114*, 9173–9177. [CrossRef]
52. Kelly, K.L.; Coronado, E.; Zhao, L.L.; Schatz, G.C. The optical properties of metal nanoparticles: The influence of size, shape, and dielectric environment. *J. Phys. Chem. B* **2003**, *107*, 668–677. [CrossRef]
53. Tian, N.; Zhou, Z.-Y.; Sun, S.-G.; Ding, Y.; Wang, Z.L. Synthesis of tetrahexahedral platinum nanocrystals with high-index facets and high electro-oxidation activity. *Science* **2007**, *316*, 732. [CrossRef] [PubMed]
54. Ming, T.; Feng, W.; Tang, Q.; Wang, F.; Sun, L.; Wang, J.; Yan, C. Growth of tetrahexahedral gold nanocrystals with high-index facets. *J. Am. Chem. Soc.* **2009**, *131*, 16350–16351. [CrossRef] [PubMed]
55. Wang, F.; Li, C.; Sun, L.-D.; Wu, H.; Ming, T.; Wang, J.; Yu, J.C.; Yan, C.-H. Heteroepitaxial growth of high-index-faceted palladium nanoshells and their catalytic performance. *J. Am. Chem. Soc.* **2011**, *133*, 1106–1111. [CrossRef]
56. Lu, B.; Liu, A.; Wu, H.; Shen, Q.; Zhao, T.; Wang, J. Hollow Au–Cu2O core–shell nanoparticles with geometry-dependent optical properties as efficient plasmonic photocatalysts under visible light. *Langmuir* **2016**, *32*, 3085–3094. [CrossRef]
57. Xia, X.; Zeng, J.; McDearmon, B.; Zheng, Y.; Li, Q.; Xia, Y. Silver nanocrystals with concave surfaces and their optical and surface-enhanced raman scattering properties. *Angew. Chem. Int. Ed.* **2011**, *50*, 12542–12546. [CrossRef]

58. Yin, P.-G.; You, T.-T.; Tan, E.-Z.; Li, J.; Lang, X.-F.; Jiang, L.; Guo, L. Characterization of tetrahexahedral gold nanocrystals: A combined study by surface-enhanced raman spectroscopy and computational simulations. *J. Phys. Chem. C* **2011**, *115*, 18061–18069. [CrossRef]
59. Rodríguez-Lorenzo, L.; Álvarez-Puebla, R.A.; Pastoriza-Santos, I.; Mazzucco, S.; Stéphan, O.; Kociak, M.; Liz-Marzán, L.M.; García de Abajo, F.J. Zeptomol detection through controlled ultrasensitive surface-enhanced raman scattering. *J. Am. Chem. Soc.* **2009**, *131*, 4616–4618. [CrossRef]
60. Hong, J.W.; Wi, D.H.; Lee, S.-U.; Han, S.W. Metal–semiconductor heteronanocrystals with desired configurations for plasmonic photocatalysis. *J. Am. Chem. Soc.* **2016**, *138*, 15766–15773. [CrossRef]
61. Simon, T.; Bouchonville, N.; Berr, M.J.; Vaneski, A.; Adrović, A.; Volbers, D.; Wyrwich, R.; Döblinger, M.; Susha, A.S.; Rogach, A.L.; et al. Redox shuttle mechanism enhances photocatalytic H2 generation on Ni-decorated CdS nanorods. *Nat. Mater.* **2014**, *13*, 1013–1018. [CrossRef]
62. Zhao, Q.; Ji, M.; Qian, H.; Dai, B.; Weng, L.; Gui, J.; Zhang, J.; Ouyang, M.; Zhu, H. Controlling structural symmetry of a hybrid nanostructure and its effect on efficient photocatalytic hydrogen evolution. *Adv. Mater.* **2014**, *26*, 1387–1392. [CrossRef] [PubMed]
63. Pan, J.; Zhang, L.; Zhang, S.; Shi, Z.; Wang, X.; Song, S.; Zhang, H. Half-encapsulated Au nanorods@CeO2 Core@Shell nanostructures for near-infrared plasmon-enhanced catalysis. *ACS Appl. Nano Mater.* **2019**, *2*, 1516–1524. [CrossRef]
64. Mubeen, S.; Lee, J.; Singh, N.; Krämer, S.; Stucky, G.D.; Moskovits, M. An autonomous photosynthetic device in which all charge carriers derive from surface plasmons. *Nat. Nanotechnol.* **2013**, *8*, 247–251. [CrossRef] [PubMed]
65. Wang, F.; Cheng, S.; Bao, Z.; Wang, J. Anisotropic overgrowth of metal heterostructures induced by a site-selective silica coating. *Angew. Chem. (Int. Ed. Engl.)* **2013**, *52*, 10344–10348. [CrossRef] [PubMed]
66. Zheng, Z.; Tachikawa, T.; Majima, T. Single-particle study of Pt-modified Au nanorods for plasmon-enhanced hydrogen generation in visible to near-infrared region. *J. Am. Chem. Soc.* **2014**, *136*, 6870–6873. [CrossRef]
67. Yang, H.; Wang, Z.-H.; Zheng, Y.-Y.; He, L.-Q.; Zhan, C.; Lu, X.; Tian, Z.-Q.; Fang, P.-P.; Tong, Y. Tunable wavelength enhanced photoelectrochemical cells from surface plasmon resonance. *J. Am. Chem. Soc.* **2016**, *138*, 16204–16207. [CrossRef]
68. Bao, Z.; Sun, Z.; Li, Z.; Tian, L.; Ngai, T.; Wang, J. Plasmonic gold−superparamagnetic hematite heterostructures. *Langmuir* **2011**, *27*, 5071–5075. [CrossRef]
69. Li, A.; Zhu, W.; Li, C.; Wang, T.; Gong, J. Rational design of yolk–shell nanostructures for photocatalysis. *Chem. Soc. Rev.* **2019**, *48*, 1874–1907. [CrossRef]
70. Fang, C.; Jia, H.; Chang, S.; Ruan, Q.; Wang, P.; Chen, T.; Wang, J. (Gold core)/(titania shell) nanostructures for plasmon-enhanced photon harvesting and generation of reactive oxygen species. *Energy Environ. Sci.* **2014**, *7*, 3431–3438. [CrossRef]
71. Ortega-Liebana, M.C.; Hueso, J.L.; Arenal, R.; Santamaria, J. Titania-coated gold nanorods with expanded photocatalytic response. Enzyme-like glucose oxidation under near-infrared illumination. *Nanoscale* **2017**, *9*, 1787–1792. [CrossRef]
72. Kou, S.F.; Ye, W.; Guo, X.; Xu, X.F.; Sun, H.Y.; Yang, J. Gold nanorods coated by oxygen-deficient TiO_2 as an advanced photocatalyst for hydrogen evolution. *RSC Adv.* **2016**, *6*, 39144–39149. [CrossRef]
73. Paier, J.; Penschke, C.; Sauer, J. Oxygen defects and surface chemistry of ceria: Quantum chemical studies compared to experiment. *Chem. Rev.* **2013**, *113*, 3949–3985. [CrossRef] [PubMed]
74. Chueh, W.C.; Falter, C.; Abbott, M.; Scipio, D.; Furler, P.; Haile, S.M.; Steinfeld, A. High-flux solar-driven thermochemical dissociation of CO_2 and H_2O using nonstoichiometric ceria. *Science* **2010**, *330*, 1797. [CrossRef] [PubMed]
75. Cargnello, M.; Jaén, J.J.D.; Garrido, J.C.H.; Bakhmutsky, K.; Montini, T.; Gámez, J.J.C.; Gorte, R.J.; Fornasiero, P. Exceptional activity for methane combustion over modular Pd@ CeO_2 subunits on functionalized Al_2O_3. *Science* **2012**, *337*, 713. [CrossRef] [PubMed]
76. Zhou, H.-P.; Wu, H.-S.; Shen, J.; Yin, A.-X.; Sun, L.-D.; Yan, C.-H. Thermally stable Pt/CeO_2 hetero-nanocomposites with high catalytic activity. *J. Am. Chem. Soc.* **2010**, *132*, 4998–4999. [CrossRef]
77. Qi, J.; Zhao, K.; Li, G.; Gao, Y.; Zhao, H.; Yu, R.; Tang, Z. Multi-shelled CeO_2 hollow microspheres as superior photocatalysts for water oxidation. *Nanoscale* **2014**, *6*, 4072–4077. [CrossRef]
78. Corma, A.; Atienzar, P.; García, H.; Chane-Ching, J.Y. Hierarchically mesostructured doped CeO2 with potential for solar-cell use. *Nat. Mater.* **2004**, *3*, 394–397. [CrossRef]

79. Jin-Ha, H.; Thomas, O.M. Defect chemistry and transport properties of nanocrystalline cerium oxide. *Z. Für Phys. Chem.* **1998**, *207*, 21–38. [CrossRef]
80. Wang, J.-H.; Chen, M.; Luo, Z.-J.; Ma, L.; Zhang, Y.-F.; Chen, K.; Zhou, L.; Wang, Q.-Q. Ceria-Coated Gold Nanorods for Plasmon-Enhanced Near-Infrared Photocatalytic and Photoelectrochemical performances. *J. Phys. Chem. C* **2016**, *120*, 14805–14812. [CrossRef]
81. Mitsudome, T.; Yamamoto, M.; Maeno, Z.; Mizugaki, T.; Jitsukawa, K.; Kaneda, K. One-step synthesis of core-gold/shell-ceria nanomaterial and its catalysis for highly selective semihydrogenation of alkynes. *J. Am. Chem. Soc.* **2015**, *137*, 13452–13455. [CrossRef]
82. Zhang, L.; Pan, J.; Long, Y.; Li, J.; Li, W.; Song, S.; Shi, Z.; Zhang, H. CeO_2-encapsulated hollow Ag–Au nanocage hybrid nanostructures as high-performance catalysts for cascade reactions. *Small* **2019**, *15*, 1903182. [CrossRef] [PubMed]
83. Luo, F.; Jia, C.-J.; Song, W.; You, L.-P.; Yan, C.-H. Chelating ligand-mediated crystal growth of cerium orthovanadate. *Cryst. Growth Des.* **2005**, *5*, 137–142. [CrossRef]
84. Kominami, H.; Tanaka, A.; Hashimoto, K. Mineralization of organic acids in aqueous suspensions of gold nanoparticles supported on cerium (iv) oxide powder under visible light irradiation. *Chem. Commun.* **2010**, *46*, 1287–1289. [CrossRef] [PubMed]
85. Kominami, H.; Tanaka, A.; Hashimoto, K. Gold nanoparticles supported on cerium (IV) oxide powder for mineralization of organic acids in aqueous suspensions under irradiation of visible light of λ = 530 nm. *Appl. Catal. A Gen.* **2011**, *397*, 121–126. [CrossRef]
86. Fasciani, C.; Alejo, C.J.B.; Grenier, M.; Netto-Ferreira, J.C.; Scaiano, J.C. High-temperature organic reactions at room temperature using plasmon excitation: Decomposition of dicumyl peroxide. *Org. Lett.* **2011**, *13*, 204–207. [CrossRef]
87. Heckert, E.G.; Seal, S.; Self, W.T. Fenton-like reaction catalyzed by the rare earth inner transition metal cerium. *Environ. Sci. Technol.* **2008**, *42*, 5014–5019. [CrossRef]
88. Kohantorabi, M.; Gholami, M.R. Fabrication of novel ternary Au/CeO2@g-C3N4 nanocomposite: Kinetics and mechanism investigation of 4-nitrophenol reduction, and benzyl alcohol oxidation. *Appl. Phys. A* **2018**, *124*, 441. [CrossRef]
89. Li, Y.; Sun, Q.; Kong, M.; Shi, W.; Huang, J.; Tang, J.; Zhao, X. Coupling oxygen ion conduction to photocatalysis in mesoporous nanorod-like ceria significantly improves photocatalytic efficiency. *J. Phys. Chem. C* **2011**, *115*, 14050–14057. [CrossRef]
90. Yin, D.; Zhao, F.; Zhang, L.; Zhang, X.; Liu, Y.; Zhang, T.; Wu, C.; Chen, D.; Chen, Z. Greatly enhanced photocatalytic activity of semiconductor CeO_2 by integrating with upconversion nanocrystals and graphene. *RSC Adv.* **2016**, *6*, 103795–103802. [CrossRef]
91. Nair, V.; Muñoz-Batista, M.J.; Fernández-García, M.; Luque, R.; Colmenares, J.C. Thermo-photocatalysis: Environmental and energy applications. *ChemSusChem* **2019**, *12*, 2098–2116. [CrossRef]
92. Italiano, C.; Llorca, J.; Pino, L.; Ferraro, M.; Antonucci, V.; Vita, A. CO and CO_2 methanation over Ni catalysts supported on CeO_2, Al_2O_2 and Y_2O_2 oxides. *Appl. Catal. B Environ.* **2020**, *264*, 118494. [CrossRef]
93. Hammedi, T.; Triki, M.; Alvarez, M.G.; Llorca, J.; Ghorbel, A.; Ksibi, Z.; Medina, F. Heterogeneous fenton-like oxidation of p-hydroxybenzoic acid using Fe/CeO_2-TiO_2 catalyst. *Water Sci. Technol.* **2019**, *79*, 1276–1286. [CrossRef] [PubMed]
94. Yang, C.; Yu, X.; Heißler, S.; Nefedov, A.; Colussi, S.; Llorca, J.; Trovarelli, A.; Wang, Y.; Wöll, C. Surface faceting and reconstruction of ceria nanoparticles. *Angew. Chem. Int. Ed.* **2017**, *56*, 375–379. [CrossRef] [PubMed]
95. Soler, L.; Casanovas, A.; Urrich, A.; Angurell, I.; Llorca, J. CO oxidation and COPrOx over preformed Au nanoparticles supported over nanoshaped CeO_2. *Appl. Catal. B Environ.* **2016**, *197*, 47–55. [CrossRef]
96. Lu, B.; Quan, F.; Sun, Z.; Jia, F.; Zhang, L. Photothermal reverse-water-gas-shift over Au/CeO_2 with high yield and selectivity in CO_2 conversion. *Catal. Commun.* **2019**, *129*, 105724. [CrossRef]
97. Ghoussoub, M.; Xia, M.; Duchesne, P.N.; Segal, D.; Ozin, G. Principles of photothermal gas-phase heterogeneous CO_2 catalysis. *Energy Environ. Sci.* **2019**, *12*, 1122–1142. [CrossRef]
98. Jantarang, S.; Lovell, E.C.; Tan, T.H.; Scott, J.; Amal, R. Role of support in photothermal carbon dioxide hydrogenation catalysed by Ni/CexTiyO_2. *Prog. Nat. Sci. Mater. Int.* **2018**, *28*, 168–177. [CrossRef]
99. Pan, Y.; Deng, S.; Polavarapu, L.; Gao, N.; Yuan, P.; Sow, C.H.; Xu, Q.-H. Plasmon-enhanced photocatalytic properties of Cu_2O nanowire–au nanoparticle assemblies. *Langmuir* **2012**, *28*, 12304–12310. [CrossRef]

100. Ren, S.; Wang, B.; Zhang, H.; Ding, P.; Wang, Q. Sandwiched ZnO@Au@Cu_2O nanorod films as efficient visible-light-driven plasmonic photocatalysts. *ACS Appl. Mater. Interfaces* **2015**, *7*, 4066–4074. [CrossRef]
101. Niu, J.; Dai, Y.; Yin, L.; Shang, J.; Crittenden, J.C. Photocatalytic reduction of triclosan on Au–Cu_2O nanowire arrays as plasmonic photocatalysts under visible light irradiation. *Phys. Chem. Chem. Phys.* **2015**, *17*, 17421–17428. [CrossRef]
102. Sharma, K.; Maiti, K.; Kim, N.H.; Hui, D.; Lee, J.H. Green synthesis of glucose-reduced graphene oxide supported Ag-Cu_2O nanocomposites for the enhanced visible-light photocatalytic activity. *Compos. Part. B Eng.* **2018**, *138*, 35–44. [CrossRef]
103. Wang, X.; Dong, H.; Hu, Z.; Qi, Z.; Li, L. Fabrication of a Cu_2O/Au/TiO_2 composite film for efficient photocatalytic hydrogen production from aqueous solution of methanol and glucose. *Mater. Sci. Eng. B* **2017**, *219*, 10–19. [CrossRef]
104. McShane, C.M.; Choi, K.-S. Photocurrent enhancement of n-type Cu_2O electrodes achieved by controlling dendritic branching growth. *J. Am. Chem. Soc.* **2009**, *131*, 2561–2569. [CrossRef] [PubMed]
105. Kong, L.; Chen, W.; Ma, D.; Yang, Y.; Liu, S.; Huang, S. Size control of Au@Cu_2O octahedra for excellent photocatalytic performance. *J. Mater. Chem.* **2012**, *22*, 719–724. [CrossRef]
106. Kuo, C.-H.; Yang, Y.-C.; Gwo, S.; Huang, M.H. Facet-dependent and Au nanocrystal-enhanced electrical and photocatalytic properties of Au−Cu_2O core−shell heterostructures. *J. Am. Chem. Soc.* **2011**, *133*, 1052–1057. [CrossRef]
107. Yuan, G.; Lu, M.; Fei, J.; Guo, J.; Wang, Z. Morphologically controllable synthesis of core–shell structured Au@Cu2O with enhanced photocatalytic activity. *RSC Adv.* **2015**, *5*, 71559–71564. [CrossRef]
108. Chiu, Y.-H.; Lindley, S.A.; Tsao, C.-W.; Kuo, M.-Y.; Cooper, J.K.; Hsu, Y.-J.; Zhang, J.Z. Hollow Au nanosphere-Cu2O core–shell nanostructures with controllable core surface morphology. *J. Phys. Chem. C* **2020**, *124*, 11333–11339. [CrossRef]
109. Kuo, C.-H.; Hua, T.-E.; Huang, M.H. Au nanocrystal-directed growth of Au−Cu_2O core−shell heterostructures with precise morphological control. *J. Am. Chem. Soc.* **2009**, *131*, 17871–17878. [CrossRef]
110. Zhang, L.; Blom, D.A.; Wang, H. Au–Cu_2O core–shell nanoparticles: A hybrid metal-semiconductor heteronanostructure with geometrically tunable optical properties. *Chem. Mater.* **2011**, *23*, 4587–4598. [CrossRef]
111. Huang, W.-C.; Lyu, L.-M.; Yang, Y.-C.; Huang, M.H. Synthesis of Cu_2O nanocrystals from cubic to rhombic dodecahedral structures and their comparative photocatalytic activity. *J. Am. Chem. Soc.* **2012**, *134*, 1261–1267. [CrossRef]
112. Xu, W.; Jia, J.; Wang, T.; Li, C.; He, B.; Zong, J.; Wang, Y.; Fan, H.J.; Xu, H.; Feng, Y.; et al. Continuous tuning of Au-Cu(2) O janus nanostructures for efficient charge separation. *Angew. Chem. (Int. Ed. Engl.)* **2020**. [CrossRef]
113. Yu, X.; Liu, X.; Wang, B.; Meng, Q.; Sun, S.; Tang, Y.; Zhao, K. An LSPR-based "push–pull" synergetic effect for the enhanced photocatalytic performance of a gold nanorod@cuprous oxide-gold nanoparticle ternary composite. *Nanoscale* **2020**, *12*, 1912–1920. [CrossRef]
114. Liu, C.; Dong, H.; Wu, N.; Cao, Y.; Zhang, X. Plasmonic resonance energy transfer enhanced photodynamic therapy with Au@SiO2@Cu2O/perfluorohexane nanocomposites. *ACS Appl. Mater. Interfaces* **2018**, *10*, 6991–7002. [CrossRef]
115. Zheng, T.; Zhou, T.; Feng, X.; Shen, J.; Zhang, M.; Sun, Y. Enhanced plasmon-induced resonance energy transfer (PIRET)-mediated photothermal and photodynamic therapy guided by photoacoustic and magnetic resonance imaging. *ACS Appl. Mater. Interfaces* **2019**, *11*, 31615–31626. [CrossRef] [PubMed]
116. Chang, Y.; Cheng, Y.; Feng, Y.; Jian, H.; Wang, L.; Ma, X.; Li, X.; Zhang, H. Resonance energy transfer-promoted photothermal and photodynamic performance of gold–copper sulfide yolk–shell nanoparticles for chemophototherapy of cancer. *Nano Lett.* **2018**, *18*, 886–897. [CrossRef] [PubMed]
117. Tao, C.; An, L.; Lin, J.; Tian, Q.; Yang, S. Surface plasmon resonance–enhanced photoacoustic imaging and photothermal therapy of endogenous H2S-triggered Au@Cu_2O. *Small* **2019**, *15*, 1903473. [CrossRef] [PubMed]
118. Wang, J.; Wu, X.; Ma, W.; Xu, C. Chiral AuCuAu heterogeneous nanorods with tailored optical activity. *Adv. Funct. Mater.* **2020**, *30*, 2000670. [CrossRef]
119. Luther, J.M.; Jain, P.K.; Ewers, T.; Alivisatos, A.P. Localized surface plasmon resonances arising from free carriers in doped quantum dots. *Nat. Mater.* **2011**, *10*, 361–366. [CrossRef] [PubMed]

120. Yu, X.; Bi, J.; Yang, G.; Tao, H.; Yang, S. Synergistic effect induced high photothermal performance of Au nanorod@Cu7S4 yolk–shell nanooctahedron particles. *J. Phys. Chem. C* **2016**, *120*, 24533–24541. [CrossRef]
121. Sun, M.; Fu, X.; Chen, K.; Wang, H. Dual-plasmonic gold@copper sulfide core–shell nanoparticles: Phase-selective synthesis and multimodal photothermal and photocatalytic behaviors. *ACS Appl. Mater. Interfaces* **2020**, *12*, 46146–46161. [CrossRef]
122. Zhang, Y.; Zhu, M.; Zhang, S.; Cai, Y.; Lv, Z.; Fang, M.; Tan, X.; Wang, X. Highly efficient removal of U(VI) by the photoreduction of SnO2/CdCO3/CdS nanocomposite under visible light irradiation. *Appl. Catal. B Environ.* **2020**, *279*, 119390. [CrossRef]
123. Yao, X.; Hu, X.; Zhang, W.; Gong, X.; Wang, X.; Pillai, S.C.; Dionysiou, D.D.; Wang, D. Mie resonance in hollow nanoshells of ternary TiO2-Au-CdS and enhanced photocatalytic hydrogen evolution. *Appl. Catal. B Environ.* **2020**, *276*, 119153. [CrossRef]
124. Kumar, S.G.; Kavitha, R.; Nithya, P.M. Tailoring the CdS surface structure for photocatalytic applications. *J. Environ. Chem. Eng.* **2020**, *8*, 104313. [CrossRef]
125. Peng, Y.; Kang, S.; Hu, Z. Pt nanoparticle-decorated CdS photocalysts for CO2 reduction and H2 evolution. *ACS Appl. Nano Mater.* **2020**, *3*, 8632–8639. [CrossRef]
126. Miodyńska, M.; Mikolajczyk, A.; Bajorowicz, B.; Zwara, J.; Klimczuk, T.; Lisowski, W.; Trykowski, G.; Pinto, H.P.; Zaleska-Medynska, A. Urchin-like TiO_2 structures decorated with lanthanide-doped Bi2S3 quantum dots to boost hydrogen photogeneration performance. *Appl. Catal. B Environ.* **2020**, *272*, 118962. [CrossRef]
127. Ji, Z.; Wang, H.; She, X. A novel CdS quantum dots decorated 3D Bi2O2CO3 hierarchical nanoflower with enhanced photocatalytic performance. *Catalysts* **2020**, *9*, 1046. [CrossRef]
128. Hou, H.; Zhang, X. Rational design of 1D/2D heterostructured photocatalyst for energy and environmental applications. *Chem. Eng. J.* **2020**, *395*, 125030. [CrossRef]
129. Karthikeyan, C.; Arunachalam, P.; Ramachandran, K.; Al-Mayouf, A.M.; Karuppuchamy, S. Recent advances in semiconductor metal oxides with enhanced methods for solar photocatalytic applications. *J. Alloys Compd.* **2020**, *828*, 154281. [CrossRef]
130. Wei, Y.; Jiao, J.; Zhao, Z.; Liu, J.; Li, J.; Jiang, G.; Wang, Y.; Duan, A. Fabrication of inverse opal TiO2-supported Au@CdS core–shell nanoparticles for efficient photocatalytic CO_2 conversion. *Appl. Catal. B Environ.* **2015**, *179*, 422–432. [CrossRef]
131. Wang, S.; Wang, X. Photocatalytic CO_2 reduction by CdS promoted with a zeolitic imidazolate framework. *Appl. Catal. B Environ.* **2015**, *162*, 494–500. [CrossRef]
132. Bak, T.; Nowotny, J.; Rekas, M.; Sorrell, C.C. Photo-electrochemical hydrogen generation from water using solar energy. Materials-related aspects. *Int. J. Hydrogen Energy* **2002**, *27*, 991–1022. [CrossRef]
133. Huang, J.; Mulfort, K.L.; Du, P.; Chen, L.X. Photodriven charge separation dynamics in CdSe/ZnS Core/Shell quantum Dot/Cobaloxime hybrid for efficient hydrogen production. *J. Am. Chem. Soc.* **2012**, *134*, 16472–16475. [CrossRef] [PubMed]
134. Xie, Y.P.; Yu, Z.B.; Liu, G.; Ma, X.L.; Cheng, H.-M. CdS–mesoporous ZnS core–shell particles for efficient and stable photocatalytic hydrogen evolution under visible light. *Energy Environ. Sci.* **2014**, *7*, 1895–1901. [CrossRef]
135. Wu, J.; Zhang, Z.; Liu, B.; Fang, Y.; Wang, L.; Dong, B. UV-Vis-NIR-driven plasmonic photocatalysts with dual-resonance modes for synergistically enhancing H2 generation. *Sol. RRL* **2018**, *2*, 1800039. [CrossRef]
136. Tang, W.; Fan, W.; Zhang, W.; Yang, Z.; Li, L.; Wang, Z.; Chiang, Y.-L.; Liu, Y.; Deng, L.; He, L.; et al. Wet/Sono-chemical synthesis of enzymatic two-dimensional MnO_2 nanosheets for synergistic catalysis-enhanced phototheranostics. *Adv. Mater.* **2019**, *31*, 1900401. [CrossRef] [PubMed]
137. Chen, W.-T.; Yang, T.-T.; Hsu, Y.-J. Au-CdS Core−Shell Nanocrystals with Controllable Shell Thickness and Photoinduced Charge Separation Property. *Chem. Mat.* **2008**, *20*, 7204–7206. [CrossRef]
138. Lee, S.-U.; Jung, H.; Wi, D.H.; Hong, J.W.; Sung, J.; Choi, S.-I.; Han, S.W. Metal–semiconductor yolk–shell heteronanostructures for plasmon-enhanced photocatalytic hydrogen evolution. *J. Mater. Chem. A* **2018**, *6*, 4068–4078. [CrossRef]
139. Li, M.; Yu, X.-F.; Liang, S.; Peng, X.-N.; Yang, Z.-J.; Wang, Y.-L.; Wang, Q.-Q. Synthesis of Au–CdS core–shell hetero-nanorods with efficient exciton–plasmon interactions. *Adv. Funct. Mater.* **2011**, *21*, 1788–1794. [CrossRef]

140. Ma, L.; Liang, S.; Liu, X.-L.; Yang, D.-J.; Zhou, L.; Wang, Q.-Q. Synthesis of dumbbell-like gold–metal sulfide core–shell nanorods with largely enhanced transverse plasmon resonance in visible region and efficiently improved photocatalytic activity. *Adv. Funct. Mater.* **2015**, *25*, 898–904. [CrossRef]
141. Chiu, Y.-H.; Naghadeh, S.B.; Lindley, S.A.; Lai, T.-H.; Kuo, M.-Y.; Chang, K.-D.; Zhang, J.Z.; Hsu, Y.-J. Yolk-shell nanostructures as an emerging photocatalyst paradigm for solar hydrogen generation. *Nano Energy* **2019**, *62*, 289–298. [CrossRef]